



A new A-type granitoid occurrence in southernmost Fennoscandia: geochemistry, age and origin of rapakivi-type quartz monzonite from the Pietkowo IG1 borehole, NE Poland

Anna Grabarczyk¹ · Janina Wiszniewska² · Ewa Krzemińska² · Zdzisław Petecki²

Received: 9 February 2022 / Accepted: 10 November 2022 / Published online: 14 January 2023
© The Author(s) 2022

Abstract

Rapakivi-type quartz monzonite and the underlying dark-grey granodiorite from the Pietkowo IG1 borehole, in the Polish part of southernmost Fennoscandia have been investigated using whole-rock geochemistry, Sm–Nd isotope geochemistry and U–Pb zircon dating. The quartz monzonite was emplaced at 1495–1491 Ma, although slightly older zircon cores (antecrysts) of 1513 Ma imply a two-stage crystallization. The geochemical similarities with Mazury Complex granitoids, their metaluminous and alkali-calcic nature, elevated contents of F, Ga and high-field-strength-elements (HFSE), indicate that the Pietkowo IG1 rapakivi-type quartz monzonite is an ‘A-type’ granitoid. The presence of magnetite and titanite indicates crystallization under oxidizing conditions. The rock is classified as A₂ sub-type, and the Nb/Y ratio implies a within-plate setting. The dark-grey granodiorite, dated to 1813 Ma, has a calc-alkaline character, typical of a volcanic-arc environment. Initial whole rock ϵ_{Nd} values range between -2.9 and -3.3 for the rapakivi-type quartz monzonite and from -1.0 to +1.1 for the dark-grey granodiorite. We suggest that the A-type Pietkowo IG1 rapakivi-type quartz monzonite was generated from the dark-grey granodiorite via partial melting at middle to lower crustal levels. The most plausible ascent route for the quartz monzonite was via lithospheric-scale weakness zones, between the eastern margin of the Mazowsze Domain and Belarus-Podlasie Granulite Belt, i.e., the Białystok fault. Therefore, the Pietkowo IG1 rapakivi-type quartz monzonite is a representative of the Mesoproterozoic A-type granitoid occurrence in southernmost Fennoscandia.

Keywords Mesoproterozoic magmatism · Pietkowo A-type quartz monzonite · Fennoscandia · U–Pb zircon ages · Sm–Nd isotopes

Introduction

A-type granites, originally distinguished by Loiselle and Wones (1979), were firstly defined as anhydrous felsic rocks with high contents of alkalis and abundant HFSE (e.g. Frost et al. 2001; Bonin 2007). Chemically A-type granites can be classified as ferroan, calc-alkaline to alkaline-calcic granitoids (Frost et al. 2001). They are inferred to occur in stable continental terranes or rift zones (Loiselle and Wones 1979;

Bonin 2007), and are commonly found within orogenic complexes that are 50–350 Ma older than A-type granitoid intrusions (Haapala and Rämö 1990), suggesting their post-orogenic nature.

A considerable number of A-type granite intrusions, commonly associated with other felsic-mafic components of the bimodal magmatism comprising anorthosites, gabbros, ferrodioritic dikes, charnockites, mangerites, etc., are present in the Laurentia and Baltica cratons (e.g. North America, Greenland, and Fennoscandian regions of Sweden, Finland and northwest Russia; Anderson and Morrison 2005). This igneous activity, known as AMCG magmatism (for anorthosite, mangerite, charnockite and granite), is restricted only to the Proterozoic Eon (Rämö et al. 1995; Frost and Frost 1997), being one of the most enigmatic episodes in Earth history.

In Fennoscandia the granitic component of the AMCG suite with characteristic rapakivi texture has been the subject

Editorial handling: L. Nasdala

✉ Anna Grabarczyk
anna.grabarczyk@uw.edu.pl

¹ Faculty of Geology, University of Warsaw, Żwirki i Wigury 93, 02-089 Warszawa, Poland

² Polish Geological Institute – National Research Institute, Rakowiecka 4, 00-975 Warszawa, Poland

of numerous petrogenetic studies. An overview has been presented by Rämö and Haapala (1995). Rapakivi granites, defined as A-type granites nowadays, form a few major exposed batholiths including the most prominent bodies of the Salmi in Russian Karelia (Fig. 1A), Riga in western Latvia (Fig. 1A) and the most classical Wiborg batholith in Finland (Fig. 1A), as well as many minor intrusions (Andersson 1997) emplaced within heterogeneous Proterozoic crust of the Baltic Shield. These types of igneous bodies have also been geophysically detected underneath platform sediments covering the southern part of the Fennoscandian block, whereas most of them have been drilled (Bogdanova et al. 2006, 2015).

A significant manifestation of AMCG magmatism is present also within the crystalline basement of northeastern Poland, near the SW margin of the East European Craton (EEC; Fig. 1A, B), constituting a complex of intrusions located latitudinally along the border between Poland, Belarus and Lithuania and known in the region as the Mazury Complex (MC). This complex is well documented by numerous drillings, therefore all AMCG members have been confirmed (Bagiński et al. 2001; Dörr et al. 2002; Skridlaite et al. 2003; Gawęda et al. 2009; Duchesne et al. 2010; Wiszniewska and Krzemińska 2021). The MC is commonly listed among other prominent examples of rapakivi-type granitoid and anorthosite massif occurrences (Rämö and Haapala 1995; Ashwal 2010; Salminen et al. 2021). Granitoids of the MC (e.g. from the Boksze 1, Krasnopol 6, Filipów 1, Łopuchowo IG1 boreholes; Fig. 1B) show features characteristic for A-type granites (Collins et al. 1982; Clemens et al. 1986; Whalen et al. 1987; Creaser et al. 1991; Rämö et al. 1995; Frost and Frost 1997).

Within the Polish crystalline basement, over 170 kmsouth of the MC, another granitoid occurrence at a depth of ~1 km has been recognized. The intrusion was first defined by regional magnetic and gravity surveys (Fig. S1; Kubicki and Ryka 1982) and drilled by the Pietkowo IG1 borehole in 1976 (Fig. 1B). The lower part of the Pietkowo IG1 profile is composed of the dark-grey granitoid (Krzemińska et al. 2007), whereas, in the upper part of the drilling granitoids (Fig. 2) with a characteristic porphyritic (rapakivi-type) texture composed of larger K-feldspar phenocrysts were found (Fig. 3E, F). This upper intrusive granitoid phase has not previously been described, but it seems to be similar to granitoids from the MC, where this texture was commonly referred to as rapakivi or rapakivi-like (Ryka and Podemski 1998; Bagiński et al. 2001).

In this contribution, we report sensitive high resolution ion microprobe (SHRIMP) U–Pb zircon ages, whole-rock geochemistry and Sm–Nd isotopic compositions for the Pietkowo IG1 igneous body. The newly obtained data are discussed together with granitoid data selected from the Mazury AMCG suite, and compared to features of classical

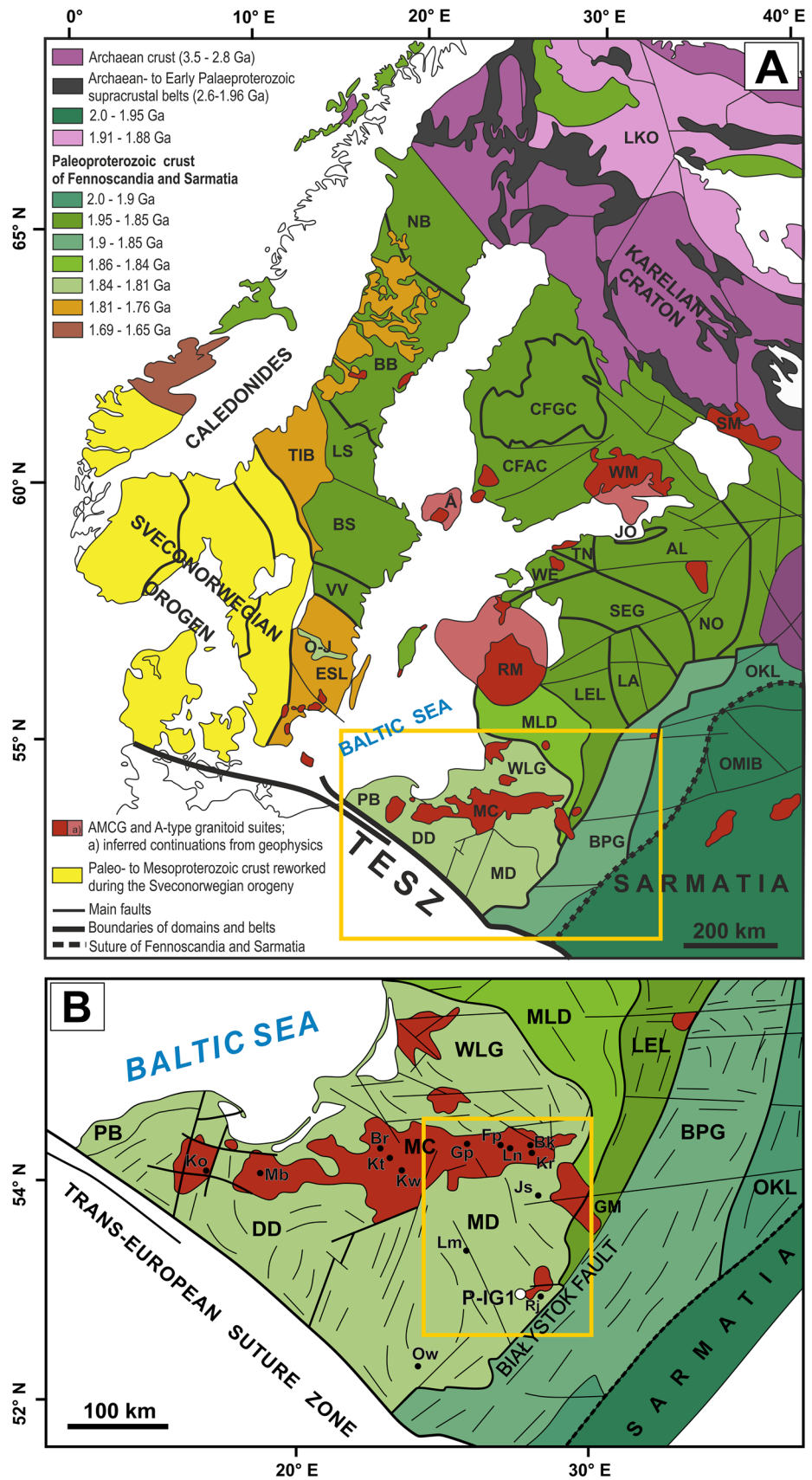
rapakivi batholiths collected from previous studies in order to assess a genetic link between Mesoproterozoic AMCG suites with A-type or ‘anorogenic’ granites, emplaced within the composite and heterogeneous Proterozoic crust of Fennoscandia during a few distinct pulses of ~1.6–1.4 Ga.

Geological setting

The EEC comprises three protocontinents: Fennoscandia, Sarmatia and Volgo-Uralia, which experienced distinct tectonic and metamorphic evolutions until their final collision at ca. 1.8 Ga (Bogdanova et al. 2015; Salminen et al. 2021). Concurrently, significant crustal growth of Fennoscandia took place during Paleoproterozoic subduction–collision episodes of the Svecofennian orogeny (Bogdanova et al. 2006, 2015). The accretion of island arcs and microcontinents led to the formation of several tectonic units with igneous ages generally decreasing towards south-southwest from 1.86 to 1.84 and 1.84–1.81 Ga to 1.81–1.76 Ga. The crystalline basement of NE Poland represents a hidden, under the Phanerozoic sedimentary strata, part of the Fennoscandian craton, located south of its exposed part in the Baltic Shield. The major tectonic units in the basement of NE Poland are the Mazowsze (MD), Dobrzyń (DD) and Pomorze-Blekinge Belt (PB) domains (Fig. 1A, B; Krzemińska et al. 2017), which extend to the SW margin of the EEC defined as the Teisseyre-Tornquist Zone (TTZ; Fig. 1A, B; Dadlez et al. 2005; Narkiewicz et al. 2015).

At ca. 1525–1500 Ma, the area of northeastern Poland was affected by intensive bimodal and multi-stage magmatism consisting of several smaller magmatic bodies (Lorenc and Wiszniewska 1999) together constituting the E-W oriented belt of the MC (Fig. 1A, B), dominated by granitoids of leucogranite to granodiorite and monzodiorite composition (Bagiński et al. 2001; Skridlaite et al. 2003; Wiszniewska et al. 2007; Duchesne et al. 2010). MC granitoids show features characteristic of A-type granites (Collins et al. 1982; Clemens et al. 1986; Whalen et al. 1987; Creaser et al. 1991; Rämö et al. 1995; Frost and Frost 1997), i.e., high potassium content and extreme enrichment in iron, resulting in high K/Na and Fe/Mg ratios, notable low H₂O content, high Ga, HFSE and rare earth element (REE) abundances, low Al, Mg, Ca, Sr, Ba and Cr concentrations, as well as the presence of the rapakivi(-like) texture (Bagiński et al. 2001; Gawęda et al. 2009; Duchesne et al. 2010). Other significant components of the MC are anorthositic-gabbroitic-noritic intrusions of the Kętrzyn, Suwałki (SAM; Fig. S1) and Sejny massifs (Wiszniewska et al. 2002). Thus, the MC is a component of the AMCG suite (Emslie 1991; Rämö and Haapala 1995). The newest U–Pb zircon SHRIMP ages indicate that rapakivi-type granitoids of the MC were intruded in

Fig. 1 **A** Major Paleoproterozoic tectonic domains of Fennoscandia (modified after Bogdanova et al. 2015). The yellow rectangle shows the area presented in Fig. 1B; **B** Geological map of the crystalline basement of NE Poland and surrounding area (modified after Bogdanova et al. 2015). The yellow rectangle shows the area presented in Fig. S1 (supplementary material). The abbreviations are: Å – Åland, AL – Alutaguse, BB – Bothnian, BS – Bergslagen, BPG – Belarus-Podlasie granulite belt, CFAS – Central Finland Arc Complex; CFGC – Central Finland Granitoid Complex, DD – Dobrzyń, ESL – East Småland, JO – Jõhvi, LA – Latgalia, LEL – Latvian-East Lithuanian, LKO – Lapland-Kola orogen, LS – Ljusdal, MC – Mazury Complex, MD – Mazowsze, MLD – Mid-Lithuanian domain, NB – Norrbotten, NO – Novgorod, O-J – Oskarshamn-Jönköping, OKL – Okolovo, OMIB – Osnitsk-Mikashevichi Igneous Belt, PB – Pomorze-Blekinge, RM – Riga massif, SEG – South Estonian granulite domain, SM – Salmi massif, TIB – Transscandinavian Igneous Belt, TN – Tallinn, VV – Västervik, WE – West Estonian domain, WLG – West Lithuanian granulite domain., WM – Wiborg massif. The abbreviations for boreholes mentioned in the text: Br – Bartoszyce IG1, Bk – Boksze PIG1, Fp – Filipów IG1, Gp – Gołdap IG1, Js – Jastrzębna IG1, Kt – Kętrzyn IG1, Kw – Klewno 1, Ko – Kościerzyna IG1, Kr – Krasnopol PIG6, Ln – Łanowicze PIG1, Lm – Łomża IG1, Mb – Malbork IG1, Ow – Okuniew IG1, P-IG1 – Pietkowo IG1, Rj – Rajsk IG1, IG3



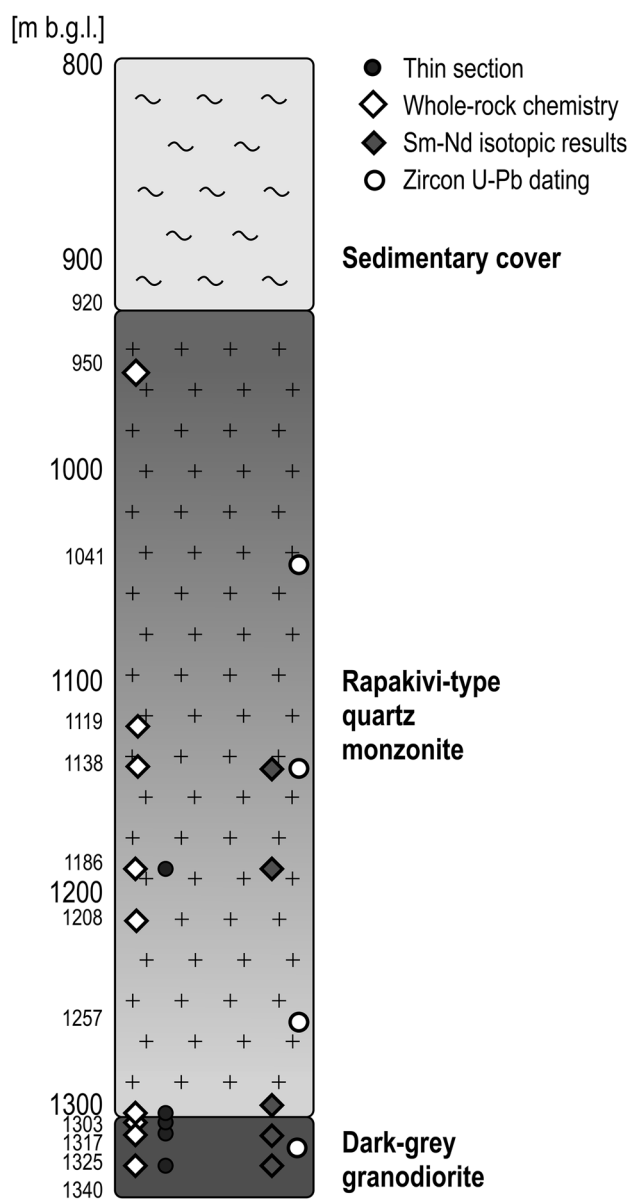


Fig. 2 Generalized lithological profile of the Pietkowo IG1 borehole, total depth of 1340 m, including the crystalline part of total thickness ~420 m. Scale in meters below ground level [m b.g.l.]. Locations of samples for EPMA study, whole-rock geochemistry, U–Pb dating and Sm–Nd isotopic investigations are shown on the profile

several magmatic pulses at 1515 Ma, 1509 Ma and 1496 Ma (Wiszniewska and Krzemińska 2021).

The new case of the rapakivi-type granitoid intrusion, drilled only by the Pietkowo IG1 borehole, is located some 170 km south of the MC and intrudes the older crystalline rocks of the MD (Fig. 1A, B). The MD generally consists of metamorphosed greywackes and shales, with intercalations of volcanogenic material. At 1830–1800 Ma metasediments were affected by bimodal magmatism examined

in, for example, the Łomża IG1, Okuniew IG1, Jastrzębna IG, Rajska IG1, Rajska IG3 and Pietkowo IG1 boreholes (Fig. 1B; Krzemińska et al. 2005, 2007; Williams et al. 2009). Therefore, they represent a classical Svecofennian sequence of low to medium grade immature metasediments, volcanogenic amphibolites and later granitoids, but slightly younger (Williams et al. 2009) than those in Scandinavia (Korja et al. 2006).

The Pietkowo IG1 borehole reaches 1340 m b.g.l. Based on lithology, it can be subdivided into three parts (Fig. 2) described below. (1) The sedimentary cover (0–920 m) is dominated by sandstones, shales and mudstones deposited in the Ediacaran to early Cambrian and in the early Triassic. The Cretaceous is composed mostly of carbonates of chalk-type facies, whereas Cainozoic strata are characterized by the presence of unconsolidated, clastic sediments (Poprawa 2019). (2) In the middle part of the profile pinkish-grey to reddish-grey porphyritic (rapakivi-type) granitoid occurs (920–1303 m; Fig. 3A–C, E, F). Its rapakivi-type texture is very similar to that observed in the MC. (3) In the last 37 m of the drill core (1303–1340 m) dark-grey medium-grained granitoids occur (Fig. 3D). They were dated to 1818 ± 15 Ma and interpreted as a representative of 1830–1800 Ma granitoids intruding the metasediments of the Svecofennian basin (Krzemińska et al. 2007). The middle part of the Pietkowo IG1 drill-section, including rapakivi-type granitoids, is the main focus of this study.

Methods of investigation

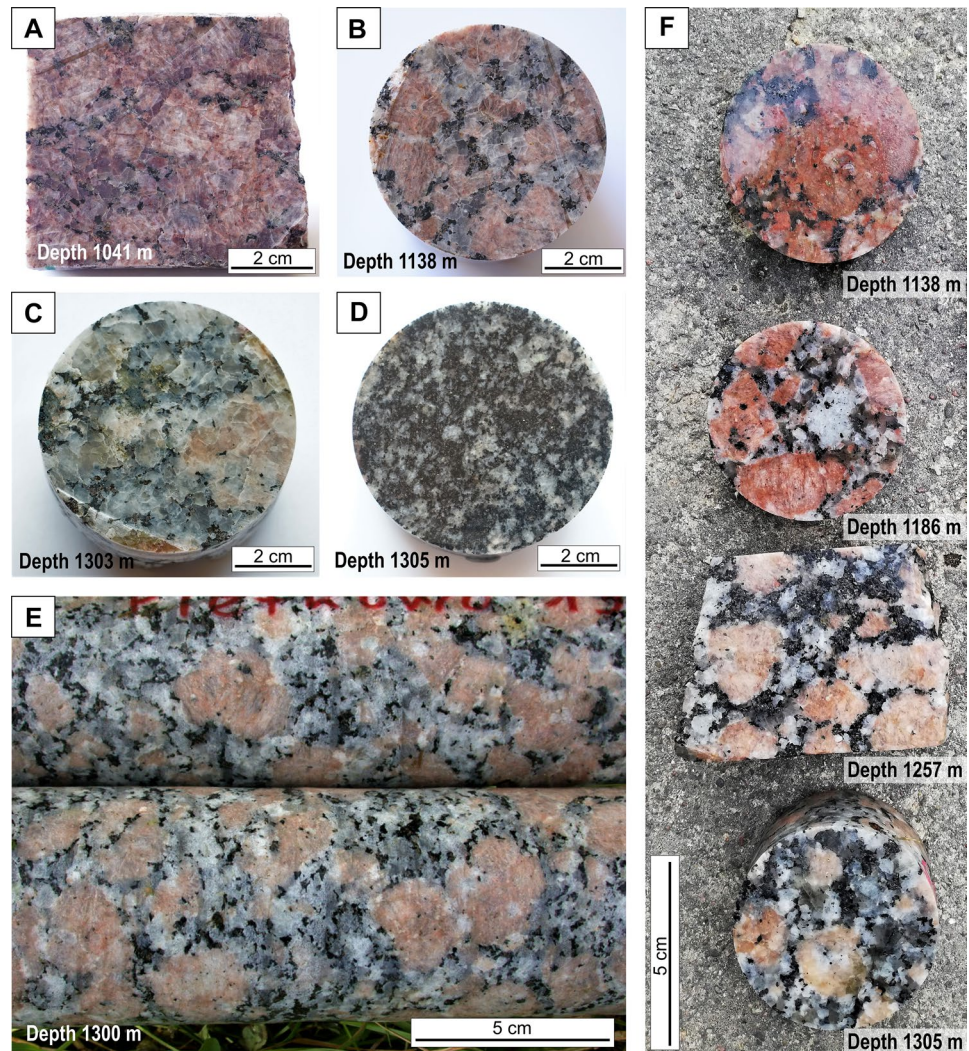
Sampling

Representative samples of the rapakivi-type granitoid and the dark-grey granitoid (Table 1) were collected from the Pietkowo IG1 drill core in the Polish Geological Institute–National Research Institute storehouse in Szurpiły. Samples of the rapakivi-type granitoid with different mineral proportions were chosen. Locations of samples for mineral chemistry, whole-rock geochemistry, zircon U–Pb SHRIMP dating and Sm–Nd isotope analysis are shown in Fig. 2.

Mineral chemistry

The chemical compositions of minerals in selected thin sections (Table 1) were investigated using the CAMECA SX-100 electron probe microanalyser (EPMA) equipped with wavelength-dispersive spectrometers (WDS). Analyses were performed under a 15 kV accelerating voltage; a 10 nA beam

Fig. 3 Macrophotographs of rocks from the Pietkowo IG1 borehole: **A** pinkish-red quartz monzonite, depth 1041 m, sample P-1041 for U–Pb dating; **B** granite with visible porphyrocrysts of pink K-feldspar forming a rapakivi-like texture, depth 1138 m, sample P-1138 for U–Pb dating and Sm–Nd isotopes analysis; **C** light-grey granite with single porphyroclasts of pinkish K-feldspar, depth 1303 m, sample P-1303a for Sm–Nd isotopes analysis; **D** fine-grained grey granodiorite of the Paleoproterozoic age, depth 1305 m, sample P-1305 for Sm–Nd isotopes analysis; **E** fragment of the Pietkowo borehole with a clearly visible rapakivi-like texture, porphyrocrysts of pinkish K-feldspar with thin oligoclase rim, depth 1300 m; **F** clear change in colour of K-feldspars with depth, from red in the upper part to light pink in the lower part, with a simultaneous decrease in the porphyritic feldspar content down the profile, samples from depths: 1138 m (P-1138 sample), 1186 m (P-1186 sample), 1257 m (P-1257 sample), 1305 m (P-1305 sample) one by one from the top



current was used for the analyses of biotite and feldspars, and 20 nA for analyses of titanite and spinel; the beam diameter ranged between focused ($\sim 1 \mu\text{m}$) and $6 \mu\text{m}$ depending on the analyzed mineral and size of analyzed grain. Reference materials and standards, selected analytical lines, diffracting crystals, peak and background counting times were as follow: Na (albite, K_{α} , TAP, 15 s, 20 s); Mg (diopside, K_{α} , TAP, 20 s, 10 s for feldspars and 30 s, 20 s for titanite); Si (diopside, K_{α} , TAP, 20 s, 10 s); Ca (diopside, K_{α} , PET, 20 s, 10 s for feldspars and 30 s, 25 s for titanite); K (orthoclase, K_{α} , PET, 20 s, 10 s); Al (orthoclase, K_{α} , TAP, 20 s, 10 s for feldspars and 30 s, 20 s for titanite); Fe (hematite, K_{α} , LIF, 40 s, 20 s); Mn (rhodonite, K_{α} , LIF, 40 s, 20 s); P (YPO_4 , K_{α} , PET, 30 s, 20 s); Ba (barite, L_{α} , LPET, 30 s, 15 s for feldspar and 60 s, 30 s for mica); Ti (rutile, K_{α} , PET, 40 s, 20 s); Zr (zircon, L_{α} , LPET, 30 s, 15 s); F (phlogopite, K_{α} , TAP, 15 s, 15 s); Sr (celestine, L_{α} , LPET, 30 s, 20 s); Y (YPO_4 , L_{α} , TAP,

30 s, 15 s); La (LaPO_4 , L_{α} , PET, 20 s, 10 s); Ce (synthetic CePO_4 , L_{α} , PET, 20 s, 10 s); Cr (synthetic Cr_2O_3 , K_{α} , LPET, 30 s, 15 s); Nb (LiNbO_3 , L_{α} , PET, 20 s, 10 s); Co (synthetic CoO , K_{α} , LIF, 30 s, 20 s); Ni (synthetic NiO , K_{α} , LIF, 30 s, 20 s); Ta (LiTaO_3 , M_{α} , TAP, 20 s, 10 s); V (V_2O_5 , K_{α} , LIF, 40 s, 20 s); Cl (tugtupite, K_{α} , LPET, 20 s, 10 s). The matrix correction was performed using the standard ZAF procedure.

Whole-rock geochemistry

Samples selected for whole-rock geochemical analyses (Table 1) were coarsely crushed by a hammer and pulverized in a corundum planetary ball-mill. Powders were subjected to a lithium borate fusion. Major elements contents were measured by means of Spectro Ciros Vision inductively coupled plasma – emission spectrometer (ICP-ES), trace elements were measured by PerkinElmer ELAN 6000

or ELAN 9000 inductively coupled plasma – mass spectrometers (ICP-MS), and F content was measured by specific ion electrode. Detection limits for each element are listed in Table 2. All analytical data were calculated on an anhydrous basis.

Sm–Nd isotope geochemistry

Samples for Nd isotopic analyses (Table 1) were ground to a fine powder with an agate mortar and pestle. Approximately 4 mg of sample powder were spiked with a mixed $^{149}\text{Sm}/^{150}\text{Nd}$ spike and dissolved with mixed HF-HNO₃ (4:1). Separation of Nd and Sm was achieved on 2 ml columns packed with Eichrom Ln resin. Details of the analytical procedure are described in Dopieralska (2003). Nd and Sm (loaded as phosphate) were measured in a Re double filament configuration. Nd was analyzed in dynamic collection mode and Sm was measured in static mode on a Finnigan MAT 261 multi-collector thermal ionization mass spectrometer. Repeated measurements of the AMES standard were conducted. Nd isotope data are reported in the standard epsilon notation (ϵ) calculated using $^{143}\text{Nd}/^{144}\text{Nd}=0.512638$ and $^{147}\text{Sm}/^{144}\text{Nd}=0.1967$ for present-day (0) chondritic uniform reservoir (CHUR₍₀₎; Jacobsen and Wasserburg 1980). All ϵ_{Nd} values are recalculated according to the measured $^{147}\text{Sm}/^{144}\text{Nd}$ ratios for the time of intrusion (t). Depleted mantle model ages (T_{DM} ; DePaolo 1981) are calculated assuming present-day depleted mantle values of $^{147}\text{Sm}/^{144}\text{Nd}=0.2137$ and $^{143}\text{Nd}/^{144}\text{Nd}=0.513151$.

U–Pb zircon geochronology

Samples for geochronological investigation were taken from the rapakivi-type granitoid from depths of 1041 m, 1138

mand 1257 m and from the dark-grey granitoid from a depth of 1317 m (Table 1). The typical procedure for zircon separation was applied. It include a sequence of steps: crushing, sieving and standard magnetic and density discrimination procedures to final hand-picking under a binocular. Extracted zircon grains were then mounted in epoxy resin together with crystals of Temora 2 and 91500 standards and polished until quasi-central sections were reached. The internal structure of the zircon grains, such as the pattern of zoning, internal domains and alteration were characterized utilizing the cathodoluminescence (CL) detector on a Hitachi SU3500 scanning electron microscope (SEM–CL). The mount surface was evaporatively coated with 10 nm Au of high purity. The U–Pb isotopic dates of selected spots on individual zircon grains were determined using the SHRIMP IIe/MC ion microprobe at the Polish Geological Institute–National Research Institute in Warsaw, Poland according to the general methodology described by Williams (1998). SHRIMP analyses were conducted using an $^{16}\text{O}^-$ primary beam. Prior to each analysis, the surface of the analysis site was pre-cleaned by rastering of the primary beam for 1.5–2 min, to reduce or eliminate surface common Pb. The sputtered area used for analysis was ca. 20–25 μm in diameter. The mass resolution was 5400 $M/\Delta M$ (at 10% peak height). During two analytical sessions on Pietkowo IG1 zircons, the count rates of nine masses were sequentially measured over 6 scans. The raw data were reduced using the SQUID Excel Macro of Ludwig (2009). The zircon U–Pb ratios were normalized relative to the Temora 2 reference zircon equivalent to $^{206}\text{Pb}^*/^{238}\text{U}=0.06683$ and age of 416.8 Ma (Black et al. 2003). The common Pb was estimated from ^{204}Pb counts. Analytical uncertainties for two sessions are given in the footnotes of Table S6 in the electronic supplementary material (ESM2). Errors given on individual analyses are

Table 1 Sampling details

Sample	Depth [m b.g.l.]	Lithology	EPMA mineral chemistry	Whole-rock chemistry	Zircon U–Pb dating	Sm–Nd isotopic results
P-950	950	QM		+		
P-1041	1041	QM			+	
P-1119	1119	QM		+		
P-1138	1138	QM		+	+	+
P-1186	1186	QM	+	+		+
P-1208	1208	QM		+		
P-1257	1257	QM			+	
P-1303a	1303	QM	+	+		+
P-1303b	1303	GD	+	+		
P-1305	1305	GD		+		+
P-1317	1317	GD			+	
P-1325	1325	GD	+	+		+

QM quartz monzonite, GD granodiorite

Table 2 Results of chemical analyses of the Mesoproterozoic rapakivi-type quartz monzonite and Paleoproterozoic dark-grey granodiorite from the Pietkowo IG1 borehole

Sample		P-950	P-1119	P-1138	P-1186	P-1208	P-1303a	P-1303b	P-1305	P-1325
Lithology	<i>DL</i>	QM	QM	QM	QM	QM	QM	GD	GD	GD
Depth		950 m	1119 m	1138 m	1186 m	1208 m	1303 m	1303 m	1305 m	1325 m
Major oxides [wt%]:										
SiO ₂	0.01	62.95	66.26	64.59	67.00	64.23	68.72	61.60	61.83	61.73
TiO ₂	0.01	0.91	0.61	0.85	0.69	0.66	0.41	0.90	0.82	0.88
Al ₂ O ₃	0.01	14.12	13.95	14.09	14.55	15.90	13.75	15.67	15.51	15.38
FeO _{tot}	0.04	4.69	3.35	4.60	4.10	3.77	5.79	6.14	5.79	6.20
MgO	0.01	1.29	0.80	1.01	0.98	0.88	0.98	2.36	2.23	2.44
MnO	0.01	0.09	0.06	0.08	0.08	0.07	0.08	0.10	0.08	0.11
CaO	0.01	2.41	2.22	2.81	2.34	2.39	3.46	4.30	4.29	4.66
Na ₂ O	0.01	2.96	3.01	3.20	2.89	2.99	3.95	2.96	3.04	2.99
K ₂ O	0.01	5.32	5.05	4.56	5.45	6.55	1.22	3.95	4.12	3.51
P ₂ O ₅	0.01	0.33	0.22	0.31	0.25	0.25	0.28	0.34	0.33	0.35
LOI	-5.1	0.80	0.60	0.50	1.30	0.70	0.90	1.40	1.70	1.40
Total		95.87	96.14	96.60	99.73	98.39	99.52	99.80	99.82	99.81
A/NK		1.33	1.34	1.38	1.37	1.32	1.76	1.71	1.64	1.76
A/CNK		0.94	0.97	0.92	0.98	0.97	0.97	0.92	0.90	0.89
Mg#		0.19	0.17	0.16	0.17	0.17	0.13	0.25	0.25	0.26
K ₂ O/Na ₂ O		1.80	1.68	1.43	1.89	2.19	0.31	1.33	1.36	1.17
FeO _t /MgO		3.23	3.72	4.05	3.72	3.81	5.25	2.31	2.26	2.31
Trace elements [ppm]:										
F		n.a	n.a	n.a	2630	n.a	2730	3230	3650	2570
Ba	1	1269	1275	1119	1223	1691	176	810	884	896
Sc	1	11.1	7.9	9.7	9.0	9.1	11.0	16.0	14.0	16.0
Co	0.2	8.0	6.0	8.0	6.0	6.0	6.7	14.8	14.2	14.1
Ga	0.5	10.0	8.0	8.0	18.3	6.0	21.0	18.7	17.4	17.8
Hf	0.1	10.0	8.0	8.0	11.3	6.0	31.9	6.3	5.7	6.5
Nb	0.1	45.0	33.0	43.0	34.5	30.0	15.4	16.9	14.8	15.0
Rb	0.1	n.a	n.a	n.a	227	n.a	85	174	169	149
Sr	0.5	347	340	351	323	414	313	429	434	397
Ta	0.1	n.a	n.a	n.a	2.3	n.a	0.9	1.0	1.2	1.0
Th	0.2	28.0	29.9	15.4	30.0	32.8	94.2	13.1	9.1	10.1
U	0.1	5.0	3.0	3.0	6.0	<2.0	5.1	2.4	3.3	1.4
V	8	51	37	52	46	42	71	101	100	105
Zr	0.1	508	372	484	474	378	1048	253	220	263
Y	0.1	76.3	52.2	69.1	53.5	52.5	27.1	24.5	22.5	21.9
La	0.1	201	169	108	159	234	532	67	51	65
Ce	0.1	448	377	298	341	485	931	137	108	124
Pr	0.02	53.0	43.8	40.2	40.1	52.5	85.5	15.6	12.6	14.3
Nd	0.3	189	151	155	145	174	242	60	49	54
Sm	0.05	31.3	23.3	27.8	21.4	24.9	20.7	10.0	8.2	8.9
Eu	0.02	5.1	3.9	4.6	3.3	4.3	2.6	1.8	1.7	1.9
Gd	0.5	20.6	15.0	18.6	14.6	15.4	11.5	7.4	6.4	6.6
Tb	0.01	2.8	1.9	2.5	1.9	2.0	1.1	0.9	0.8	0.9
Dy	0.05	15.3	10.5	14.1	10.1	11.0	5.4	4.8	4.3	4.5
Ho	0.02	2.8	1.9	2.6	2.0	2.0	0.9	0.9	0.8	0.8
Er	0.03	7.8	5.4	7.1	5.3	5.4	2.7	2.4	2.3	2.3
Tm	0.01	1.1	0.7	1.0	0.8	0.7	0.4	0.3	0.3	0.3
Yb	0.05	6.6	4.6	6.0	5.1	4.4	2.8	2.0	2.0	1.8
Lu	0.01	0.9	0.7	0.8	0.7	0.6	0.5	0.3	0.3	0.3

Table 2 (continued)

Sample	P-950	P-1119	P-1138	P-1186	P-1208	P-1303a	P-1303b	P-1305	P-1325
Lithology	<i>DL</i>	QM	QM	QM	QM	QM	GD	GD	GD
Depth	950 m	1119 m	1138 m	1186 m	1208 m	1303 m	1303 m	1305 m	1325 m
Total REE	984	808	686	750	1015	1839	310	247	285
Y/Nb	1.70	1.58	1.61	1.55	1.75	1.76	1.45	1.52	1.46
Yb/Ta	-	-	-	2.20	-	3.14	1.98	1.64	1.83
(La/Sm) _N	4.03	4.57	2.44	4.68	5.91	16.18	4.20	3.93	4.55
(Eu/Yb) _N	2.19	2.42	2.21	1.86	2.77	2.63	2.60	2.41	2.92
(La/Yb) _N	20.5	24.8	12.2	21.1	36.0	126.7	22.7	17.5	23.8
Eu/Eu*	0.61	0.64	0.62	0.58	0.67	0.52	0.65	0.71	0.77
T _{Zr}	870	849	864	872	843	963	n.a	n.a	n.a

QM quartz monzonite, GD granodiorite, DL detection limits, LOI loss on ignition, A/CNK Al₂O₃/(CaO+Na₂O+K₂O) molar; A/NK Al₂O₃/(Na₂O+K₂O) molar; #mg MgO/(MgO+FeO), Eu/Eu* [Eu_N/√(Sm_N×Gd_N)], N chondrite (C1) normalized to values of Boynton (1984), n.a. not analysed

based on counting statistics and are at the 1 sigma. Errors for pooled analyses are at 2 sigma. The ages and errors of intercepts of the best-fit line with concordia were calculated using the Isoplot program (Ludwig 2003). The mean square of weighted deviates (MSWD) and probability of fit values are given in the text and on the concordia diagrams. Throughout two analytical sessions, Temora 2 zircons were analyzed every three sample spots provided mean ²⁰⁶Pb/²³⁸U ages of 416.7 ± 2.9 Ma (n = 15) and 416.8 ± 1.9 Ma (n = 20), accurate to reference values (²⁰⁶Pb/²³⁸U age of 416.78 ± 0.33 Ma) of Black et al. (2004) obtained by thermal ionization mass spectrometry (TIMS). As a comparison, the U–Th–Pb results previously obtained from one dark-grey granitoid sample, depth 1317 m (Krzemińska et al. 2007), were also attached. This sample was only briefly presented in the form of an abstract without analytical data. This zircon sample (depth 1317 m) was analyzed on SHRIMP II ion microprobe at the Australian National University in Canberra, Australia based on techniques described by Williams (1998). In the present contribution the data were re-calculated again using Isoplot program (Ludwig 2003).

Results

Petrography and mineral compositions

Rapakivi-type granitoid

The rapakivi-type granitoid shows a porphyritic non-oriented texture with feldspar megacrysts (~2–3 cm) embedded in a finer-grained groundmass. A few ovoidal megacrysts are partially mantled by a thin shell of creamy plagioclase, however, most of them do not develop the plagioclase mantles (Fig. 3E, F). The rapakivi-type granitoid does not show a

uniform phase composition through the Pietkowo IG1 profile. There is a clear change in color of alkali feldspars with depth (Fig. 3F), from red in the upper part of the profile (P-950, P-1041, P-1119, P-1138, P-1186 samples) to light pink in its lower part (P-1208, P-1257, P-1303a samples).

Samples from the upper part of the profile show a relatively high content of alkali feldspar (30–40 vol%), with quartz content of 20–30 vol% and plagioclase of 35 vol%. Phenocrysts of red alkali feldspar show compositions from Or₈₈ to Or₉₇ with an Ab content up to 12 mol% (Table S1; Fig. S2A). The concentration of Ba in alkali feldspar is low (0.3–0.6 wt%; Cs_{0.6–1.1}; Fig. S2C). Alkali feldspar contains perthitic exsolutions, which show a widespread composition of An_{3–27} with an Or content up to 6.30 mol% (Table S2; Fig. S2A). The plagioclase is oligoclase, with an An content between 17 and 28 mol% (Table S2; Fig. S2A). Plagioclase grains show slight oscillatory zoning, with more calcic cores (An₂₈) and sodic rims (An_{22–25}). Iron is usually responsible for the red color of alkali feldspars, but the Fe content is low and does not exceed 0.16 wt% FeO (Fig. S2B).

Samples from the lower part, compared to granitoid samples from the upper part, are characterized by a definitely lower content of alkali feldspar (20–30 vol%), with, however, a very similar composition of Or 93–96 mol% and Ab 4–8 mol%. Moreover, these samples have a high content of plagioclase (ca. 40 vol%) and quartz (25–35 vol%). Plagioclase grains display a diverse composition, from oligoclase to andesine, with An content between 19 and 44 mol% (Table S2; Fig. S2A), with a tendency to a more calcic core (An = 27–44 mol%) and sodic rim (An = 19–26 mol%). Down the profile the FeO content in plagioclase decreases and in the P-1303a sample does not exceed 0.13 wt%.

F-rich biotite (mostly 2.02–3.01 wt% F) is the only mafic mineral with a constant content through the profile of the rapakivi-type granitoid (ca. 5 vol%). It is classified as phlogopite (Table S3; Fig. S2D) and displays very limited Fe/

(Fe + Mg) ratios of 0.44–0.47. With no evidence of chloritization, it commonly contains abundant apatite and zircon inclusions. Phlogopite exhibits rather low Ti contents in the range of 1.09–1.80 wt% TiO₂. Titanite, in both the upper and lower part of the profile, is present as subhedral crystals, up to 2 mm in size. It has TiO₂ contents within the narrow range of 29.9–31.8 wt% and is rich in Al₂O₃ (4.2–5.8 wt%) and F (1.07–3.60 wt%). Nb and Ta contents of 0.20–0.56 wt% Nb₂O₅ and 0.15–0.40 wt% Ta₂O₅ are notable (Table S4). Titanite probably does not contain a significant H₂O content, as suggested by EPMA microanalyses with totals near 100 wt%. The rapakivi-type granitoid is rich in coarse interstitial magnetite grains of amoeboid shape. The content of Ti is usually below the detection limit, whereas Cr and V concentrations do not exceed 0.04 wt% and 0.26 wt%, respectively (Table S5). Abundant apatite and zircon, as well as epidote and allanite, are present as accessory minerals.

Dark-grey granitoid

The dark-grey granitoid is moderately deformed, with an oriented fabric at the bottom part of the drilled sequence. It is macroscopically uniform – equigranular, medium-grained and felsic, with occasional larger grains of plagioclase (Fig. 3D) or alkali feldspar. The dark-grey granitoid has a constant mineral composition with ca. 30 vol% of quartz, 15 vol% of alkali feldspar and ca. 25 vol% of plagioclase. Biotite is abundant (ca. 15 vol%), definitely more common than in the rapakivi-type granitoid. The rock contains also small amounts of amphibole (hornblende; Krzemińska et al. 2007). Accessory minerals include titanite, apatite, zircon and Fe-Ti oxides.

Alkali feldspar, with a composition similar to this from the rapakivi-type granitoid (Or₈₈ to Or₉₇; Table S1, Fig. S2A, C), contains 0.46–1.30 wt% BaO (Cs_{0.8–2.4}).

Plagioclase is An_{22–40} (Table S2; Fig. S2A). However, the composition of larger plagioclase does not vary significantly (An_{33–40, 30–35}) within one grain. Plagioclase in the groundmass is more sodic, An_{22–23}.

Phlogopite (Table S3; Fig. S2D), with Fe/(Fe + Mg) = 0.45–0.50, contains 0.78 to 1.53 wt% F. It has a low Ti content of 1.43–1.84 wt% TiO₂. Phlogopite, with no evidence of chloritization, commonly contains abundant apatite and zircon inclusions.

Euhedral titanite crystals, up to 2 mm long, contain 35.1–37.6 wt% TiO₂. Al₂O₃ concentrations do not exceed 2.2 wt%. Titanite has lower Fe (1.1–2.4 wt% Fe₂O₃), Nb (up to 0.27 wt% Nb₂O₅) and Ta (0.16–0.33 wt% Ta₂O₅) compared to this hosted in the rapakivi-type granitoid (Table S4).

Magnetite is slightly enriched in Cr (up to 0.28 wt%), V (up to 0.36 wt%) and Ti (up to 0.30 wt%; Table S5). Some magnetite grains mantled large titanite.

Geochemistry

Preliminary data for the chemical composition of the dark-grey granitoid from the Pietkowo IG1 borehole were published by Krzemińska et al. (2007), however, no whole-rock chemical analyses were performed for the rapakivi-type granitoid. New whole-rock geochemical analyses for both rock types are shown in Table 2.

The rapakivi-type granitoid, with a high alkali sum of 7.8–9.5 wt% (Na₂O + K₂O) at SiO₂ contents of 63.0–68.7 wt% (Table 2; Fig. 5E), is quartz monzonite according to the total alkali-silica (TAS) diagram of Middlemost (1994). MgO and total FeO (FeO_T) contents are 0.80–1.29 wt% and 3.35–5.79 wt%, respectively (Table 2; Fig. 5A, B), whereas the Mg# (Mg/(Mg + Fe²⁺)) values are within the range of 0.13–0.19. The rapakivi-type quartz monzonite is metaluminous, with Aluminous Saturation Index (A/CNK = molar ratio of Al₂O₃/(CaO + Na₂O + K₂O)) ranging from 0.92 to 0.98 (Fig. 4A). Following the Frost et al. classification (2001), most samples are ferroan and magnesian and alkalic to calc-alkalic (Fig. 4B, C). Slightly different whole-rock chemical composition shows sample P-1303a – with higher FeO_T and CaO contents it is calcic. This sample has a lower alkali content (5.79 wt%) and on the TAS diagram plots in the granodiorite field. The F contents in the rapakivi-type quartz monzonite range from 2630 to 2730 ppm (Table 2). On major element Harker diagrams (Fig. 5) the rapakivi-type quartz monzonite forms common trends with other granitoids of the MC, but have much higher silica contents. For most major elements, there is a clear link between the content of individual elements and the content of SiO₂. The reverse relationship between SiO₂ and Fe, Mg, Ti and P (Fig. 5A, B, D, F) may indicate the liquid line of descent trend. Trace elements from the rapakivi-type quartz monzonite show negative correlation for Nb, Y, Zr, V (Fig. 6A, D, E, F) and Th and La (not shown) against SiO₂. The quartz monzonite exhibits relative depletions in Sr (313–414 ppm), Zr (372–1048 ppm) and V (37–71 ppm) compared to MC granitoids. Noteworthy, all these trends are disturbed by the P-1303a sample with lower Nb and Y and higher Nd, Zr, La, Th and V contents.

The dark-grey granitoid has SiO₂ of ca. 62 wt% (Table 2), Na₂O + K₂O of 6.5–7.2 wt% (Fig. 5E) and plots in the granodiorite field on the TAS diagram (Middlemost 1994). The Mg# is distinctly higher than for the rapakivi-type quartz monzonite (Mg# = 0.25–0.26), with higher MgO and FeO_T contents in the ranges of 2.23–2.44 wt% and 5.79–6.20 wt% (Table 2; Fig. 5A, B), respectively, and FeO_T/MgO of 2.26–2.31. The dark-grey granodiorite samples are magnesian (Fig. 4B) and are metaluminous with the A/CNK ratio between 0.89 and 0.92 (Table 2; Fig. 4A). The dark-grey granodiorite, with the CaO content of 4.29–4.66

wt%, (Fig. 5C) plots in the calc-alkalic field (Frost et al. 2001; Fig. 4C). The concentrations of F are relatively high (2570–3650 ppm).

Chondrite-normalized REE patterns (Boynton 1984) for both the rapakivi-type quartz monzonite and the dark-grey granodiorite, as well as a field with value ranges for MC granitoids, are shown in Fig. 7A. The REE patterns for the rapakivi-type quartz monzonite are similar, showing a uniform REE distribution, except for sample P-1303a, which has a significantly higher REE content (1839 ppm) than other samples ($\sum\text{REE} = 686\text{--}1015$ ppm). The majority of samples exhibit steep patterns for light rare earth elements (LREE) and moderately steep to almost flat for heavy rare earth elements (HREE), showing well-defined fractionation trends for LREE with $(\text{La}/\text{Sm})_{\text{N}} = 2.4\text{--}5.9$, and moderately trends for HREE with $(\text{Eu}/\text{Yb})_{\text{N}} = 1.9\text{--}2.8$ ($(\text{La}/\text{Yb})_{\text{N}} = 12.2\text{--}36.0$). All samples show negative Eu/Eu* anomalies (0.58–0.67). Sample P-1303a exhibits a different fractionation trend with $(\text{La}/\text{Yb})_{\text{N}} = 126.7$ and $(\text{La}/\text{Sm})_{\text{N}} = 16.2$, and simultaneously, a flat HREE pattern. In general, REE patterns for the Pietkowo IG1 rapakivi-type quartz monzonite are comparable to the MC granitoid patterns.

A characteristic feature of the dark-grey granodiorite is lower REE concentrations in the range of 247–310 ppm. Compared to the rapakivi-type quartz monzonite, dark-grey granodiorite samples have almost identical fractionation patterns with $(\text{La}/\text{Sm})_{\text{N}} = 3.9\text{--}4.6$ and $(\text{Eu}/\text{Yb})_{\text{N}} = 2.4\text{--}2.9$ ($(\text{La}/\text{Yb})_{\text{N}} = 17.5\text{--}23.8$). The dark-grey granodiorite shows negative Eu anomalies, with $\text{Eu}/\text{Eu}^* = 0.65\text{--}0.75$ (Fig. 7A).

The trace element patterns of both rock types are presented on the primitive mantle-normalized (Sun and McDonough 1989) multi-element diagram (Fig. 7B). Trace element signatures confirm the homogenous nature for both rock types (except the P-1303a sample). All samples are

enriched, to varying degrees, in large-ion lithophile elements (LILE) and in HFSE compared to the primitive mantle. They display patterns with pronounced negative anomalies for Nb, Sr, P and weaker negative anomalies for Ti and Zr in the case of the dark-grey granodiorite. These negative anomalies reflect the fractionation of plagioclase, apatite, and Fe–Ti oxides during earlier stages of magma evolution.

Geochronology

General remarks

Zircons were selected from the rapakivi-type quartz monzonite samples from depths of 1041 (Fig. 3A; P-1041 sample), 1138 (Fig. 3B, F; P-1138 sample) and 1257 (Fig. 3F; P-1257 sample) m. The set of grains consists of large euhedral grains with concentric zonation, where cores and rims are distinguished based on distinct brightness in the CL imaging (Fig. S3A–F). Inherited cores or metamorphic overgrowths are absent. Most likely, this type of zonation documents prolonged and, in places, disturbed magmatic crystallization of a granitic rock.

Pietkowo IG1; 1041 m

Twenty-five analyses on 24 grains were performed, four of them (Table S6) providing discordant results (% disc. > 5). The accepted single spot $^{207}\text{Pb}/^{206}\text{Pb}$ ages gave a wide range between 1561 ± 37 Ma (+4% disc.) and 1453 ± 22 (-4% disc.). The most consistent group of analyses ($n = 12$) is represented by the outer fragments of zircon grains, which yielded the concordia age of 1495 ± 4 Ma with $\text{MSWD} = 0.45$ (Fig. 8A). This age is interpreted as close to the emplacement age of the rapakivi-type quartz monzonite.

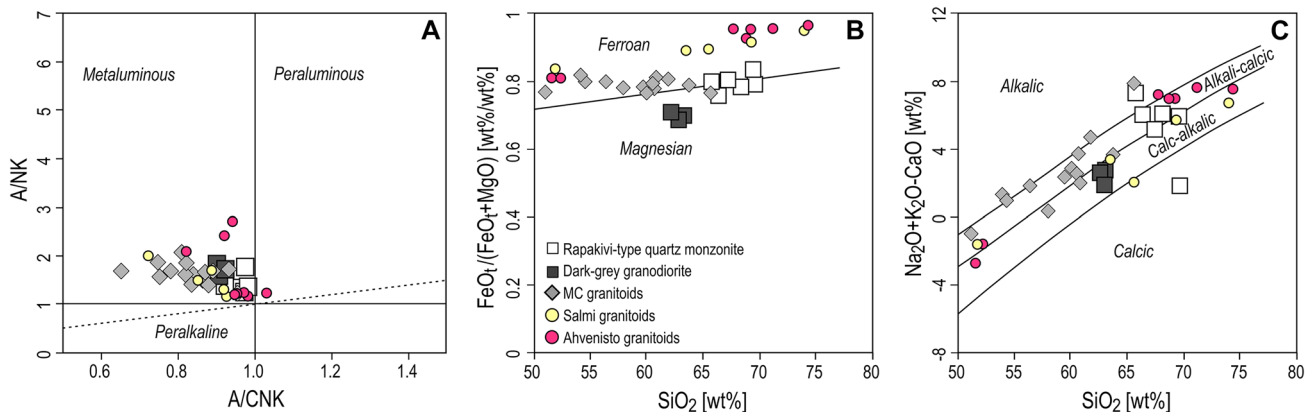
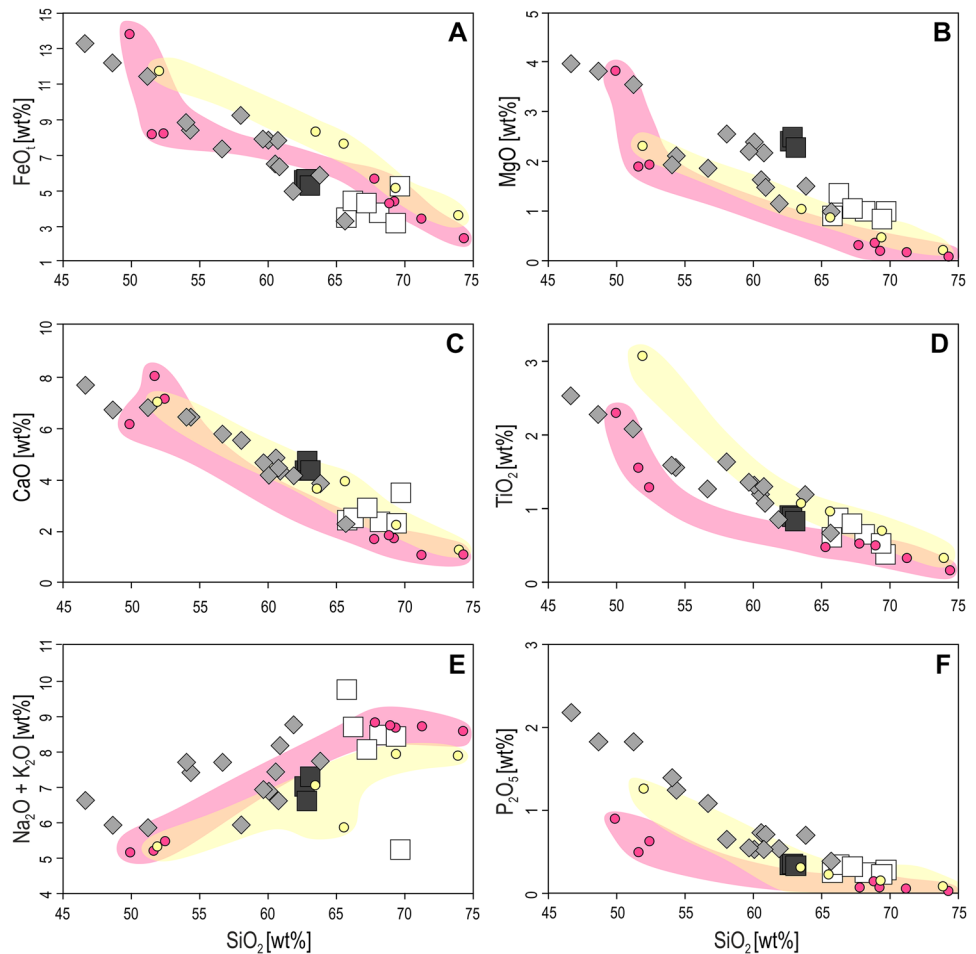


Fig. 4 Discrimination diagrams for the rapakivi-type quartz monzonite and dark-grey granodiorite: **A** $\text{Al}_2\text{O}_3/(\text{Na}_2\text{O} + \text{K}_2\text{O})$ versus $\text{Al}_2\text{O}_3/(\text{CaO} + \text{Na}_2\text{O} + \text{K}_2\text{O})$ molar diagram (after Shand 1943); **B** $\text{FeO}_t/(\text{FeO}_t + \text{MgO})$ versus SiO_2 diagram (after Frost et al. 2001);

C $\text{Na}_2\text{O} + \text{K}_2\text{O} - \text{CaO}$ versus SiO_2 diagram (after Frost et al. 2001). Data for MC granitoids after Duchesne et al. (2010), for the Salmi massif after Sharkov (2010) and for the Ahvenisto massif after Heinonen et al. (2010b)

Fig. 5 Selected variation diagrams of major element compositions against silica for whole-rock samples of the rapakivi-type quartz monzonite and the dark-grey granodiorite. Data for MC granitoids after Duchesne et al. (2010), for the Salmi massif after Sharkov (2010) and for the Ahvenisto massif after Heinonen et al. (2010b). Same symbols as in Fig. 4



Zircon has a Th/U ratio of 0.6–1.35 (Fig. 9A, B), and U and Th concentrations of 20–197 ppm and 18–126 ppm, respectively.

Pietkowo IG1; 1138 m

Twenty-six analyses on 24 grains were carried out. Only two (Table S6), with slightly discordant ages (% disc. +6 and -6% respectively), have been omitted, providing single spot ²⁰⁷Pb/²⁰⁶Pb ages ranging from 1558 ± 31 Ma (+1% disc.) to 1461 ± 18 Ma (-3% disc.). These data overlap ages obtained on the P-1041 sample. The most consistent group of n = 14 grains yielded a concordia age of 1492 ± 5 Ma with MSWD = 1.3 (Fig. 8B). This age is interpreted as the emplacement age of the rapakivi-type quartz monzonite. Zircon data, with U = 22–222 ppm and Th = 16–108 ppm, plot at Th/U ratio of 0.38–1.39 (Fig. 9A, B).

Pietkowo IG1; 1257 m

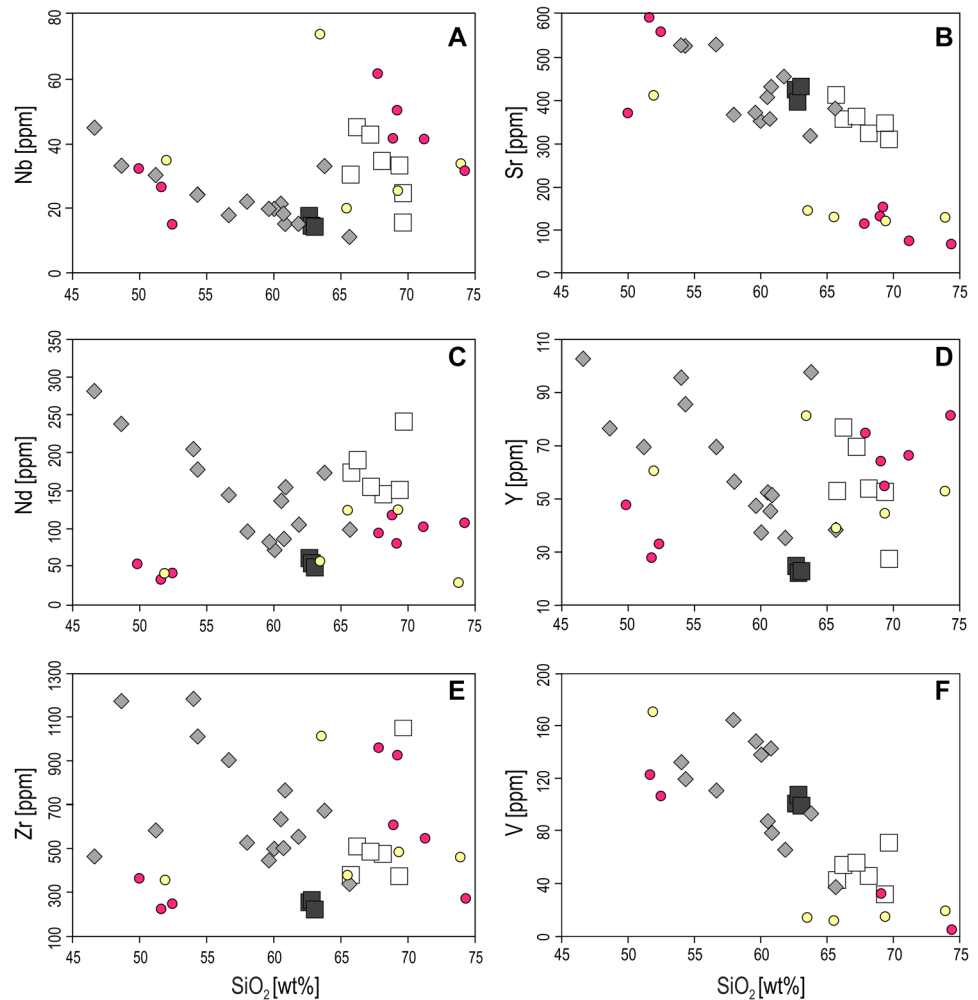
Zircon grains from sample P-1257, chosen for the ion microprobe age determination, in places show microcracks previously not observed in the CL imaging. Grains are prismatic

with a typical magmatic zonation and some structural perturbations within the central part of grains (Fig. S3E, F). U and Th concentrations range between 39–247 ppm and 28–280 ppm, respectively, giving the Th/U ratio of 0.47–1.46 (Fig. 9A, B). Thirty-six measurements on 33 zircon grains within cores and outer parts were performed. Twelve analyses, with discordance > 5%, were excluded from the dataset, giving twenty-four analyses for further interpretation (Table S6). The single spot ²⁰⁷Pb/²⁰⁶Pb ages of that group reflect a wide range between 1542.5 ± 18 Ma (+2% disc.) and 1437 ± 24 (+3% disc.). The most consistent group, representing the outer fragments of grains (n = 11), yielded a concordia age of 1491 ± 5 Ma with MSWD = 0.64 (Fig. 8C). This is interpreted as close to the emplacement age of the quartz monzonite. The limited number of results from the cores of larger grains provided a concordia age at 1513 ± 7 Ma (MSWD = 0.74; Fig. 8D).

Pietkowo IG1; 1317 m

The set of zircon grains from the dark-grey granodiorite, depth 1317 m, are euhedral prisms with length ca. 180–250 μm. The sample consists of simple melt-precipitated

Fig. 6 Selected variation diagrams of trace element compositions against silica for whole-rock samples of the rapakivi-type quartz monzonite and the dark-grey granodiorite. Data for MC granitoids after Duchesne et al. (2010), for the Salmi massif after Sharkov (2010) and for the Ahvenisto massif after Heinonen et al. (2010b). Same symbols as in Fig. 4

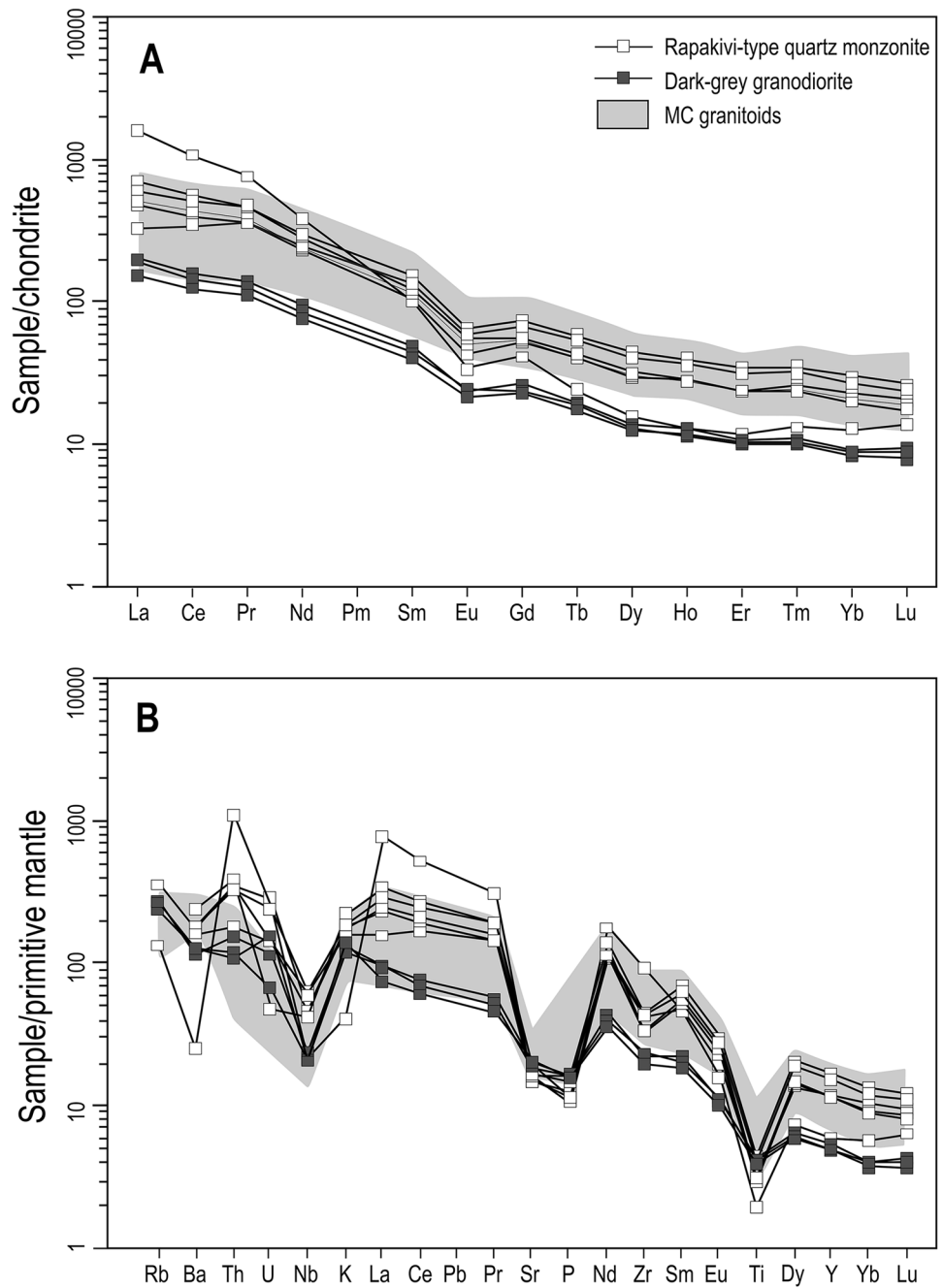


grains. The absence of inherited cores or metamorphic overgrowths was confirmed by the SEM-CL imaging (Fig. S3G, H). The zircon grains from this sample were analyzed in 2005 and described by Krzemińska et al. (2007). The analytical data have been recalculated. U contents range from 166 to 701 ppm and Th from 107 to 397 ppm. The Th/U ratio is in the range of 0.43–1.05 (Fig. 9A, B) and is typical of magmatic zircons. Single spot $^{207}\text{Pb}/^{206}\text{Pb}$ ages ($n=8$) ranged from 1827 ± 16 Ma to 1732 ± 30 Ma. The inset shows two results differing slightly from the main group, suggesting a younger population (Fig. 8E), although other parameters such as Th/U ratio and contents of Th, U, Pb do not distinguish these zircons. Five from eight analyses define the concordia age of 1813 ± 11 Ma (MSWD=0.34; Fig. 8F), which reflects the time of zircon magmatic protolith crystallization. This age is consistent with a previously published result of 1818 ± 15 Ma. The omitted younger zircons do not form a significant group; however the age of these grains corresponds to the activity (at 1758 ± 15 Ma), which has been much better documented in the Mid-Lithuanian Domain (MLD; Fig. 1A, B; Skridlaite et al. 2021).

Sm–Nd isotopes

Samples of the Mesoproterozoic rapakivi-type quartz monzonite and the Late Paleoproterozoic dark-grey granodiorite were analyzed for the Sm and Nd isotope composition (Table 3). These two groups have distinct Nd and Sm concentrations. The rapakivi-type quartz monzonite has higher amounts of Nd, ranging from 118.15 ppm to 266.68 ppm and Sm, from 22.01 ppm to 37.77 ppm, resulting in $^{147}\text{Sm}/^{144}\text{Nd}$ ratios between 0.0856 and 0.1126. Present-day ϵ_{Nd} values range between -19.35 and -24.15. The initial ϵ_{Nd} values show a narrow range between -2.95 and -3.31 (Fig. 10). Corresponding T_{DM} ages, following the model of DePaolo (1981), fall between 2.07 and 2.25 Ga and calculated chondritic uniform reservoir model ages (T_{CHUR}) fall between 1.70 and 1.80 Ga (Table 3). In the case of the dark-grey granodiorite the measured Nd and Sm concentrations and isotope values are much more uniform. Nd and Sm contents are 80.1–83.1 ppm and 13.2–14.5 ppm, respectively, resulting in $^{147}\text{Sm}/^{144}\text{Nd}$ ratios of 0.0997 and 0.1052. Present-day ϵ_{Nd}

Fig. 7 **A** C1 chondrite-normalized (Boynton 1984) rare-earth element patterns and; **B** primitive mantle-normalized (Sun and McDonough 1989) trace element patterns for the rapakivi-type quartz monzonite and the dark-grey granodiorite



have values of -21.42 and -22.26. The initial ϵ_{Nd} show near-chondritic values of -0.99 and 1.14 (Fig. 10). Corresponding T_{DM} model ages, following the model of DePaolo (1981), were calculated as 2.14 and 2.31 Ga and T_{CHUR} model ages gave values of 1.72 and 1.90 Ga. The isotope characteristics do not show any obvious correlation between Nd isotope values and SiO_2 content (Fig. 6C), but the higher Sm–Nd isotope composition of the Mesoproterozoic rapakivi-type quartz monzonite samples points to their high values of La and in consequence strong enrichment in LREE and the sum of REE (Table 2).

Discussion

Classification

Although Mesoproterozoic granitoids of the MC, known from deep boreholes in the north easternmost basement of Poland, do not show all features of the classical rapakivi texture, they were, however, placed on the ‘*Global map and list of rapakivi granite-gabbro-anorthosite complexes known by 1993*’ published by Mineralogy and Petrology (Rämö and Haapala

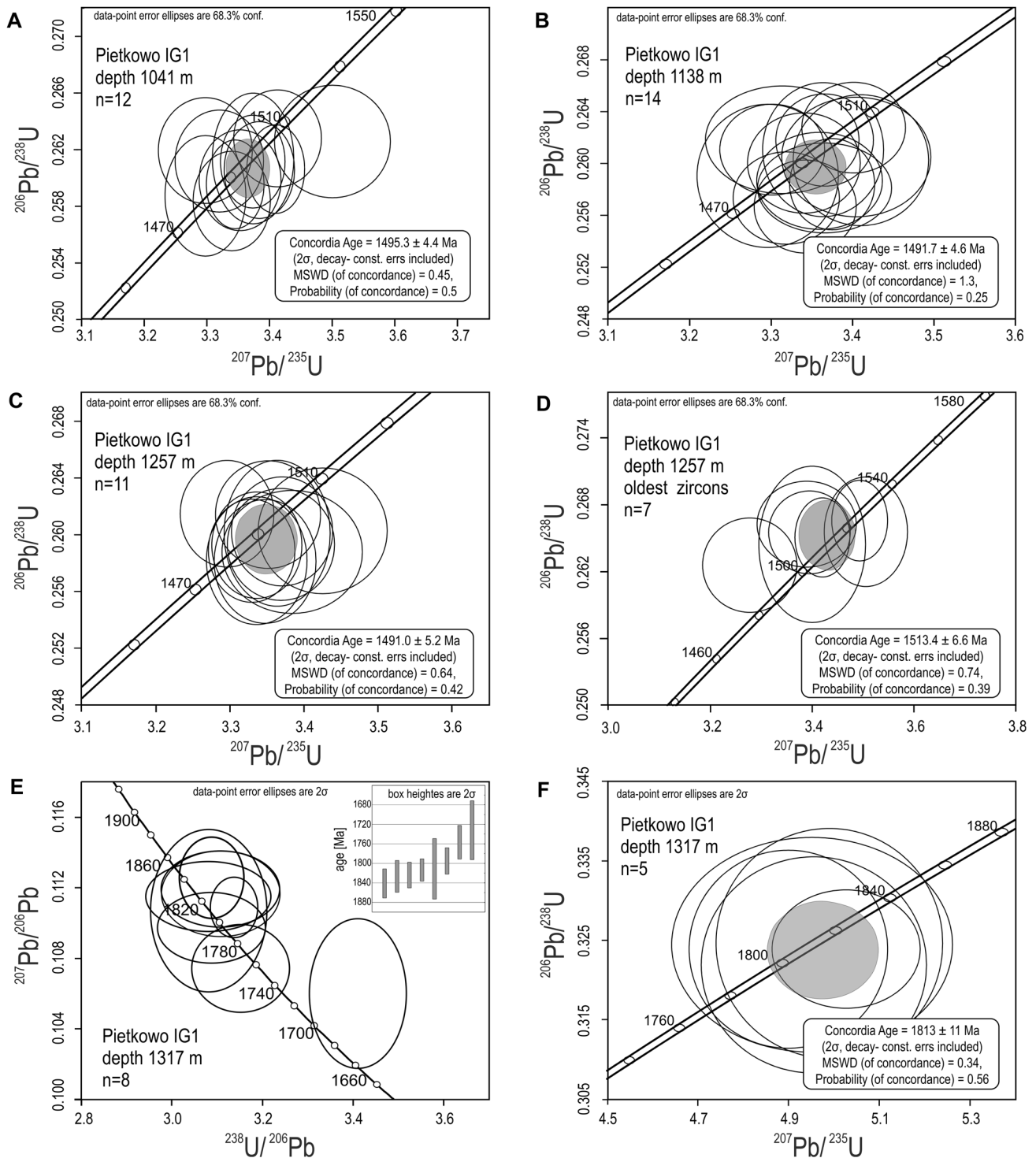


Fig. 8 Wetherill plots for selected analyses with defined concordia ages for zircon grains separated from Pietkowo IG1 rapakivite-type quartz monzonite; **A** zircon grains from P-1041 sample, depth 1041 m; **B** zircon grains from P-1138 sample, depth 1138 m; **C** zircon grains from P-1257 sample, depth 1257 m; **D** older zircon grains from P-1257 sample, depth 1257 m. Plots for analyses of

zircon grains separated from Pietkowo IG1 dark-grey granodiorite; **E** $^{207}\text{Pb}/^{206}\text{Pb}$ age projection for all collected analyses of zircon grains from P-1317 sample, depth 1317 m; **F** concordia age (recalculated) for selected analyses of zircon grains from P-1317 sample, depth 1317 m

1995). Most of presented therein Fennoscandian cases (11/13) were related to easily accessible areas of the Baltic Shield. Over the past three decades the list has undoubtedly been expanded (cf. Salminen et al. 2021), but does not yet include the Pietkowo IG1 quartz monzonite from the hidden part of Fennoscandia, which is characterized by the presence of texture resembling this of rapakivi-type granites (Fig. 3E, F). To determine potential analogues, the whole-rock compositional data of the Pietkowo IG1 rapakivi-type quartz monzonite were compared to granitoids from the MC (i.e. Bartoszyce, Gołdap, Filipów, Klewno and Kętrzyn boreholes; Fig. 1B; Duchesne et al. 2010) and two classical rapakivi A-type granite batholiths i.e., the Salmi in Russian Karelia and the Ahvenisto (satellite of the Wiborg massif) in S Finland (Fig. 1A).

The Mesoproterozoic Pietkowo IG1 quartz monzonite displays unequivocal features of A-type granites (cf. Collins et al. 1982; Whalen et al. 1987; Eby 1992; King et al. 1997; Frost et al. 2001). It has high contents of incompatible elements of the HFSE group, e.g., Nb, Zr, Y, Th (Table 2; Fig. 6A, D, E), plotting within the range of A-type granites in the $\text{FeO}_t + \text{MgO}$ versus $\text{Zr} + \text{Nb} + \text{Ce} + \text{Y}$ and Zr versus $10000 \times \text{Ga}/\text{Al}$ of Whalen et al. (1987) diagrams (Fig. 11A, B), together with granitoids of the Salmi and Ahvenisto (Heinonen et al. 2010b; Sharkov 2010) used as the most representative data for A-type rapakivi batholiths. On the Nb-Y-Ce diagram (Eby 1992) the Pietkowo rapakivi-type quartz monzonite, together with Salmi and Ahvenisto granitoids, plots in the A_2 field (Fig. 11C). The Pietkowo IG1 samples are classified as metaluminous but close to the peraluminous border, with an alkali-calcic nature, which corresponds to the main trend of the compositions known from the Salmi, Ahvenisto, and MC granitoids (Fig. 4A, C). Only the Fe and Mg contents show some differences. Instead of the unequivocally ferroan characteristics of the Salmi and Ahvenisto, the Pietkowo IG1 quartz monzonite displays a transitional nature, plotting on the border between ferroan and magnesian type, which coincides with a part of the MC data (Fig. 4B).

In terms of tectonic setting the high Nb and Y concentrations of the Pietkowo IG1 quartz monzonite indicate a typical within-plate granite (WPG) geochemical signature (Pearce et al. 1984), where they overlap with available data from the intraplate MC, Salmi and Ahvenisto batholiths, and fall into the overall 'post-collisional' field (Fig. 11D).

The A-type granites of the Laurentia–Baltica cratons have been commonly subdivided into three groups: ilmenite, magnetite and two-mica (peraluminous) granites (cf. Ishihara 1977; Anderson and Morrison 2005; Dall'Agnol and de Oliveira 2007). The Pietkowo IG1 quartz monzonite belongs to the typical magnetite-series, i.e., the $\text{Fe}/(\text{Fe} + \text{Mg})$ ratios in the biotite are low, ranging from 0.44 to 0.47 (Table S3) and the whole-rock ratio of $\text{FeO}_t/(\text{FeO}_t + \text{MgO})$ is between 0.76 and 0.84 (Table 2; Fig. 11E; cf. Dall'Agnol and de Oliveira 2007). The observed slight negative Eu anomaly suggests oxidizing

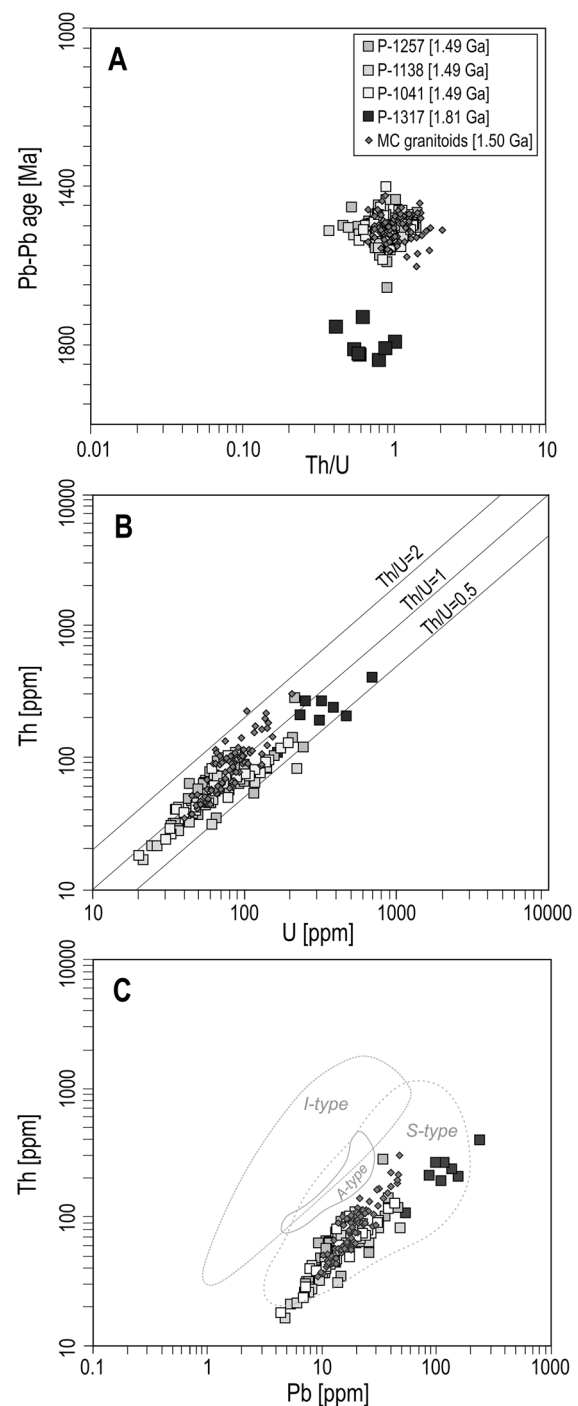


Fig. 9 The age and Th-U composition of individual zircons from Pietkowo rocks: A Pb-Pb age versus Th/U diagram; B Th versus U diagram for all zircons, showing a predominance of zircons with magmatic origin; C Th versus Pb diagram defining zircon from A-, S- and I-type granites after Wang et al. (2012). Note that Pietkowo IG1 and MC granitoid zircons are shifted toward values of S-type granites, which may be caused by the accuracy of the Pb determinations depending on the method – secondary ion mass spectrometry (SIMS) for Pietkowo IG1 and MC zircons and laser ablation–inductively coupled plasma–mass spectrometry (LA-ICP-MS) for zircons from Wang et al. (2012)

conditions of crystallization (Dall'Agnol et al. 2005) rather than the lack of earlier feldspar fractionation. Noteworthy, the ubiquitous occurrence of magnetite and titanite indicates that the Pietkowo IG1 quartz monzonite has an oxidized character as do other magnetite-series granites (Wones 1989; Rajesh 2000; Rämö et al. 2002; Dall'Agnol and de Oliveira 2007), as increases in fO_2 favor titanite stability (Price et al. 1999). Thus, the rapakivi-type quartz monzonite, most likely, crystallized near or slightly above the Ni–NiO (NNO) buffer (Rajesh 2000). The oxidized nature is also shown on the diagram of Dall'Agnol and de Oliveira (2007), where the Pietkowo IG1 quartz monzonite contrasts with reduced A-type granites of the Salmi and Ahvenisto batholiths. The same oxidized character was previously reported for MC granitoids (Duchesne et al. 2010). However, in the case of the MC it was concluded that two different sources, with different H_2O content, provided parental magmas.

In order to characterize zircons from the Pietkowo IG1 Mesoproterozoic quartz monzonite the new data have been compiled with trace elements data reported by previous workers (Dörr et al. 2002; Wiszniewska and Krzemińska 2021). The analyzed zircons from Pietkowo IG1 quartz monzonite samples exhibit Th/U ratios similar to those from MC granitoids (Fig. 9A, B). In contrast, total U and Th trace element contents tend to be higher in zircons from the Late Paleoproterozoic dark-grey granodiorite sample (Fig. 9B). The relations between Pb against Th concentrations in zircons remain similar (Fig. 9C), giving a consistent group of plots. Systematically, the data from the Pietkowo IG1 quartz monzonite and MC granitoids differ from the range of the A-type classification field, defined by Wang et al. (2012). This case however, points more likely to the crustal signature of the melt but not the S-type character of the granite host rock (Fig. 9C).

Petrogenesis

Origins proposed for A-type granites (both oxidized and reduced) essentially are associated with crustal anatexis promoted by magmatic underplating (Rämö et al. 1995; Dall'Agnol et al. 1999a, 2005). Preferred sources vary from melt-depleted granulite (Collins et al. 1982; Clemens et al. 1986; Whalen et al. 1987), granodiorite-tonalite-quartz diorite (Creaser et al. 1991; Emslie 1991; King et al. 1997; Patiño Douce 1997; Dall'Agnol et al. 1999a) to underplated tholeiitic basalts and their differentiates (Frost and Frost 1997; Frost et al. 1999). Nevertheless, fractional crystallization from alkaline basalts (Eby 1992) or other mantle-derived magmas (Bonin 2007) has also been proposed for the origin of A-type granites. Thus, it is obvious that the A-type granitoid group may contain felsic rocks of a variety of compositions, which depend on several factors, including the source nature, the pressure of melting, fO_2 conditions, and water content related to the composition of the magma source or sources depending also on changes in conditions (Dall'Agnol and de Oliveira 2007; Duchesne et al. 2010).

Nevertheless, the oxidized nature of the Pietkowo IG1 quartz monzonite argue against a tholeiitic source since partial melting of basalts and their differentiates would produce rather reduced magmas (Frost and Frost 1997). A La/Y versus La diagram (not shown) suggests an overall partial melting as the main mechanism of A-type magma formation. Therefore, the partial melting of crustal rocks is the preferred genetic model for the A-type Pietkowo IG1 quartz monzonite.

Most authors point towards a lower crustal source for oxidized A-type granites (Clemens et al. 1986; Creaser et al. 1991; Landenberger and Collins 1996; Anderson and Morrison 2005; Dall'Agnol and de Oliveira 2007). However, the generation

Table 3 Sm–Nd isotopic results for the Mesoproterozoic rapakivi-type quartz monzonite and Paleoproterozoic dark-grey granodiorite from the Pietkowo IG1 borehole

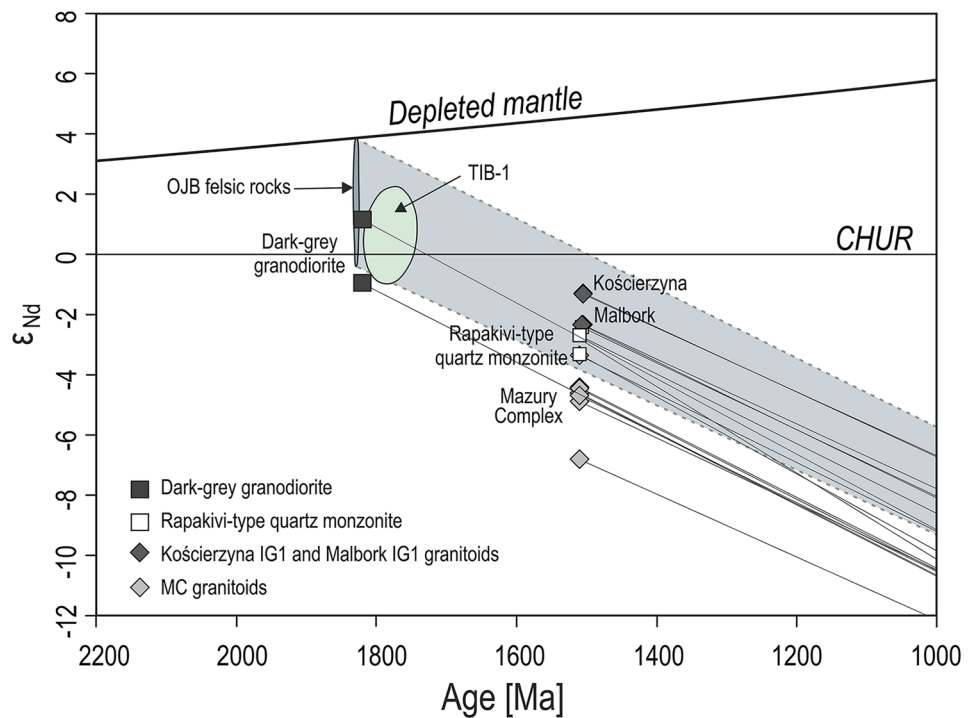
Sample	Nd [ppm]	Sm [ppm]	Sm/Nd	$^{143}\text{Nd}/^{144}\text{Nd}$ (0) measured	$\epsilon_{\text{Nd}(0)}$	Age [Ma]	$^{143}\text{Nd}/^{144}\text{Nd}$ (0)	$\epsilon_{\text{Nd}(0)}$ ^a	$^{147}\text{Sm}/^{144}\text{Nd}$	T_{DM} ^b [Ga]	T_{CHUR} ^c [Ga]
P-1138	266.68	37.77	0.14	0.511400 ± 10	–24.15	1492 Ma	0.5106	–2.95	0.0856	2.07	1.70
P-1186	118.15	22.01	0.19	0.511646 ± 11	–19.35	1492 Ma	0.5105	–3.31	0.1126	2.25	1.80
P-1303a	211.45	31.49	0.15	0.511438 ± 10	–23.41	1492 Ma	0.5106	–3.05	0.0900	2.10	1.71
P-1305	80.08	13.20	0.16	0.511540 ± 15	–21.42	1813 Ma	0.5104	1.14	0.0997	2.14	1.72
P-1325	83.12	14.46	0.17	0.511497 ± 13	–22.26	1813 Ma	0.5102	–0.99	0.1052	2.31	1.90

^a $\epsilon_{\text{Nd}(0)}$ values were calculated using $^{143}\text{Nd}/^{144}\text{Nd}=0.512638$ and $^{147}\text{Sm}/^{144}\text{Nd}=0.1967$ in the present (0) chondrite (Jacobsen and Wasserburg 1980)

^b T_{DM} depleted mantle Nd model age

^c T_{CHUR} chondritic uniform reservoir model age

Fig. 10 ϵ_{Nd} evolution diagrams for the rapakivi-type quartz monzonite and the dark-grey granodiorite. The dark-grey granodiorite in relation to evolution trends for OJB (Oskarshamn-Jönköping Belt) and TIB-1 (Transscandinavian Igneous Belt). The Mesoproterozoic rapakivi-type quartz monzonite in comparison to Kościerzyna, Malbork and MC granitoids. Sources of data: OJB and TIB-1 rocks fields after Appelquist et al. (2011), MC granitoids after Duchesne et al. (2010); Kościerzyna and Malbork granitoids after Krzemińska et al. (2017). Depleted mantle curve from DePaolo (1981)



of Pietkowo IG1 A-type melts as a consequence of partial melting probably took place at a relatively shallow depth (< 30 km), under low pressure (ca. 500–700 MPa), which is shown by relationships between $\text{Al}_2\text{O}_3/(\text{FeO} + \text{MgO} + \text{TiO}_2)$ versus $\text{Al}_2\text{O}_3 + \text{FeO} + \text{MgO} + \text{TiO}_2$ on Patiño Douce (1999) diagram (Fig. 11F). Similar melting conditions were proposed by Creaser et al. (1991), who modelled the melt formation at 600–800 MPa – characteristic of middle to lower crust. This is consistent with experimental studies conducted by Patiño Douce and Beard (1995), who concluded that, in oxidizing conditions, melts generated by dehydration melting at lower pressures (≤ 4 kbar) should be enriched in Al_2O_3 compared to those melts formed at more elevated pressures. This is in contrast to alumina behavior in reduced A-type granite (Patiño Douce 1997). The Pietkowo IG1 quartz monzonite contains 13.8–15.9 wt.% Al_2O_3 , while in most A-type granites alumina contents range from 11 to 14 wt.% Al_2O_3 (cf. Eby 1990; King et al. 1997; Dall’Agnol and de Oliveira 2007). Note that MC granitoids exhibit Al_2O_3 concentrations of 13.9–17.7 wt.% (Duchesne et al. 2010).

Oxidized A-type granites are considered to crystallize from magmas with appreciable water contents. Dall’Agnol and de Oliveira (2007) inferred H_2O content on ≥ 4 wt%, whereas the experimental studies of Clemens et al. (1986) and Dall’Agnol et al. (1999b) gave 2.4–4.3 and 4.5–6.5 wt% H_2O in the melt, respectively.

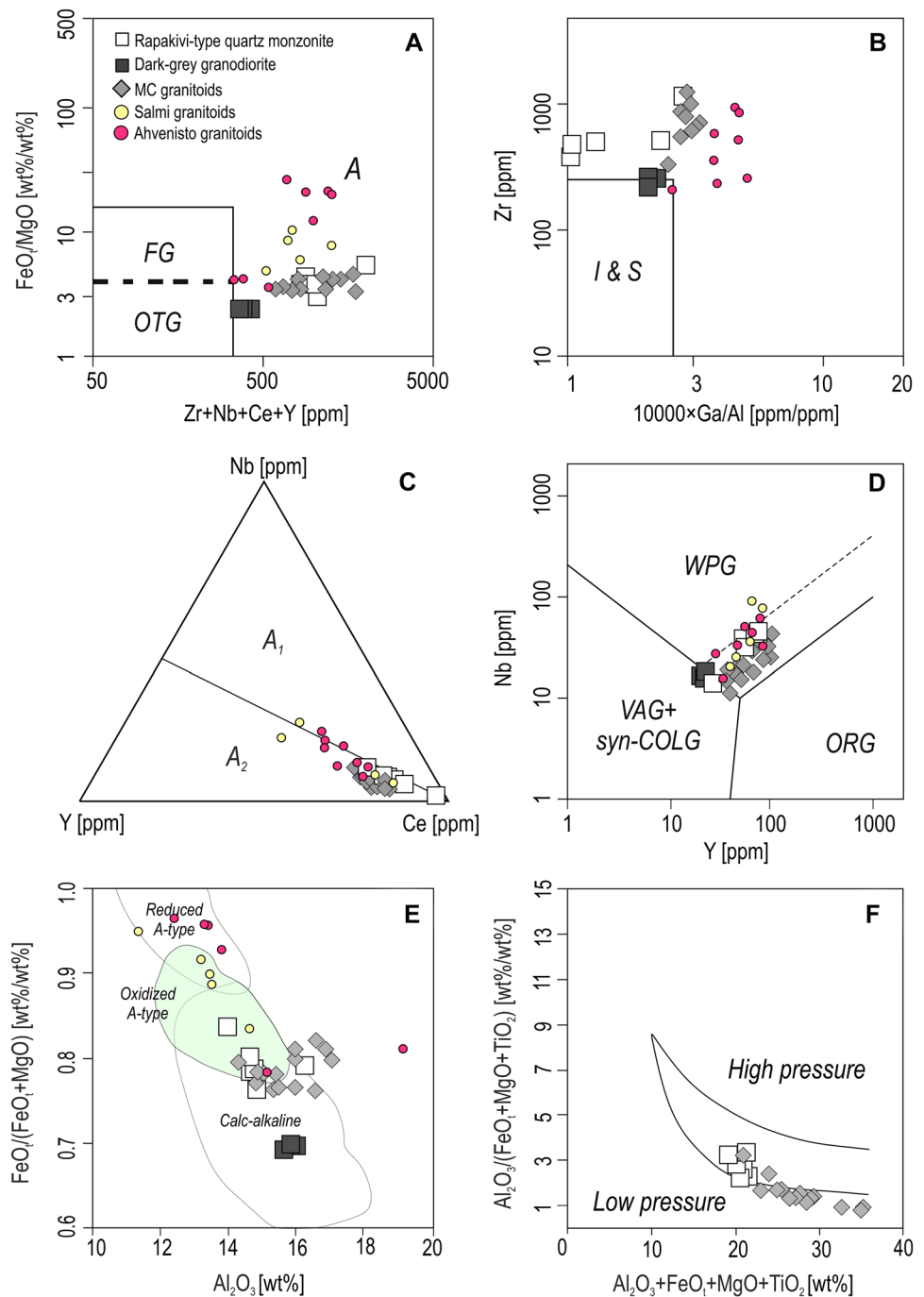
Moreover, A-type granitic magmas are usually regarded as evolving at elevated temperatures (e.g. Collins et al. 1982; Clemens et al. 1986; Creaser et al. 1991; King et al. 1997;

Dall’Agnol et al. 1999b). The zircon saturation temperature > 840 °C calculated from the whole-rock composition of the Pietkowo IG1 rapakivi-type quartz monzonite may support this tendency (Table 2), however this temperature rather indicates a potential condition for initiation of crystallization.

This study deals with rapakivi texture rocks, which are a special subgroup of A-type granites (Haapala and Rämö 1992). The common alkali feldspar megacrysts, which occur in Pietkowo IG1 quartz monzonite, are difficult to interpret unambiguously. In very general terms, the rapakivi texture was referred to in connection with magma mixing (Słaby et al. 2002; Heinonen et al. 2017) or as an effect of decompression and undercooling during magma ascent and two stage crystallization (Heinonen et al. 2017). In most cases, formation of the rapakivi texture was dominated by changes in the intensive parameters (P – T) of the magmatic system during ascent of crystal saturated magma from mid crustal levels to superficial chambers (Eklund and Shebanov 1999; Heinonen et al. 2017).

One of the features of rapakivi texture formed during decompression should be a small compositional change between the first and second generations of feldspars (Bladh 1980), and zircon and mafic silicates in different textural positions (Eklund and Shebanov 1999). The zircon data from the Pietkowo IG1 rapakivi may suggest complex crystallization representing an early stage of slow crystallization in deep magma chambers (antecrysts with a concordant age of 1513 ± 7 Ma) and, second, with much smaller, anhedral

Fig. 11 Geochemical classification of the dark-grey granodiorite and the rapakivi-type quartz monzonite together with a comparison with MC granitoids (Duchesne et al. 2010), Salmi granitoids (Sharkov 2010) and Ahvenisto granitoids (Heinonen et al. 2010b): **A, B** FeO_1/MgO versus $\text{Zr} + \text{Nb} + \text{Ce} + \text{Y}$ and Zr versus $10000 \times \text{Ga}/\text{Al}$ diagrams defining I, M, S and A-type granitoids, from Whalen et al. (1987); **C** diagram defining the A_1 and A_2 subtypes of the A-type granites using Nb–Y–Ce after Eby (1992); **D** tectonic discrimination diagram using Nb versus Y after Pearce et al. (1984): WPG – within-plate granites, VAG – volcanic arc granites, syn-COLG – syn-collisional granites, ORG – oceanic ridge granites, post-COLG – post-collisional granites; **E** diagram defining calc-alkaline and A-type granites with reduced and oxidized subtypes fields, from Dall’Agnol and de Oliveira (2007); **F** $\text{Al}_2\text{O}_3/(\text{FeO}_1 + \text{MgO} + \text{TiO}_2)$ versus $\text{Al}_2\text{O}_3 + \text{FeO}_1 + \text{MgO} + \text{TiO}_2$ diagram defining the fields of the low pressure ($P \leq 500$ MPa) and high pressure ($P = 1.2\text{--}1.5$ GPa) of the melt generation, from Patiño Douce (1999)



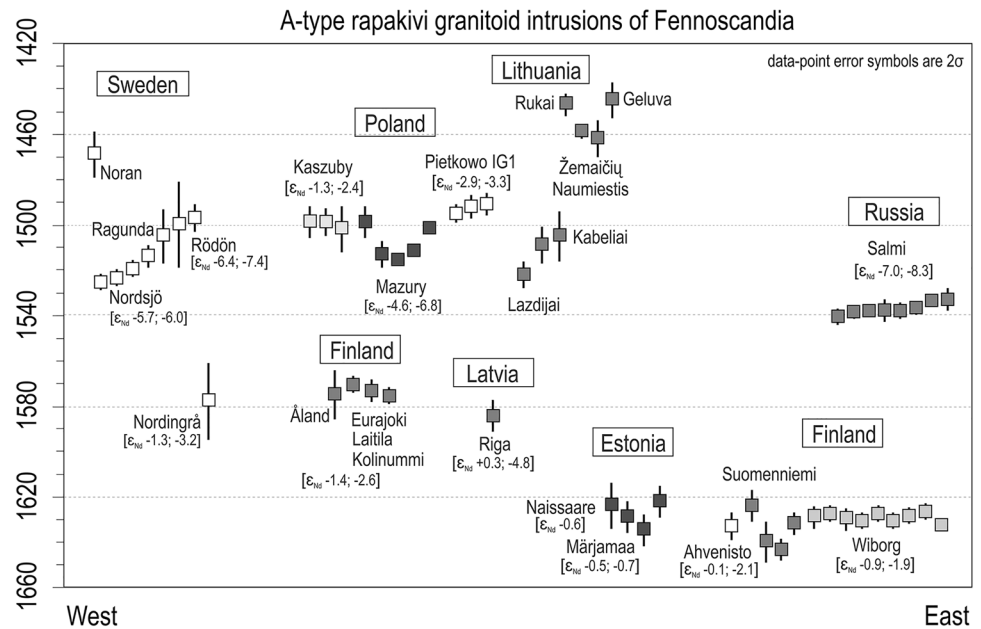
crystals or rims that crystallized at the final intrusion level at 1495–1491 Ma. A two-stage magmatic evolution was recently documented by a zircon study from the Wiborg rapakivi batholith (Heinonen et al. 2017), and by zircons from the MC AMCG suite (Wiszniewska and Krzemińska 2021).

In most cases, the isotopic composition of rapakivi granites is compatible with a lower crustal, early Proterozoic (and/or Archean) protolith (Rämö and Hoppala 1995). In terms of Nd isotopes, the Pietkowo IG1 quartz monzonite T_{DM} ages of 2.07–2.25 Ga (Table 3) are, in general,

similar to those of the Late Paleoproterozoic dark-grey granodiorite ($T_{\text{DM}} = 2.14\text{--}2.31$ Ga). Moreover, the quartz monzonite falls within the upper (more radiogenic) part of the evolution field of the dark-grey granodiorite, which indicates that the A-type quartz monzonite has been generated through melting of the dark-grey granodiorite with a little or no input of mantle-derived magmas.

Melting of the dark-grey granodiorite is also suggested by the Y/Nb ratio, which, due to melting, undergoes little change from the calc-alkaline source rock (Y/Nb ratio

Fig. 12 Compilation diagram showing the emplacement ages and whole-rock initial ϵ_{Nd} values for the AMCG complexes of central and southern Fennoscandia. ϵ_{Nd} data from: this study [Pietkowo], Duchesne et al. 2010; Wiszniewska and Krzemińska 2021 and ref. therein [Mazury], Krzemińska et al. 2021 [Kaszuby], Rämö et al. 1996 [Riga, Märjamaa, Naissaare], Neymark et al. 1994 [Salmi], Rämö et al. 2014; Heinonen et al. 2010a [Wiborg], Fröjdö et al. 1996 [Nordingrå], Heinonen et al. 2010a [Eurajoki, Kolinummi], Rämö 1991 [Åland], Heinonen et al. 2010b [Ahvenisto], Andersson et al. 2001 [Rödön, Nordsjö]



of 1.5 for the Paleoproterozoic dark-grey granodiorite) to derived melt ($Y/Nb = 1.6\text{--}1.8$ for the Mesoproterozoic rapakivi-type quartz monzonite) fingerprinting the source (Table 2; Eby 1990). The rapakivi-type quartz monzonite Y/Nb ratios of 1.6–1.8 and Yb/Ta ratios of 2.2–3.1 are characteristic of crustal values (Eby 1990). Also, the lack of an obvious correlation between Nd isotopic values and SiO_2 content suggests a limited role for assimilation/contamination, while the oxidized affinity of the rapakivi-type quartz monzonite is difficult to reconcile with the contribution of metasedimentary wall rocks (Dall'Agnol et al. 2005; Jiang et al. 2011).

An origin of the Pietkowo rapakivi-type quartz monzonite by melting of the dark-grey granodiorite is also supported by the relatively high content of F (2630–2730 ppm) in the quartz monzonite melt, as during melting of the granodiorite source the breakdown of phlogopite and amphibole would provide F to the melt. Higher F contents of 2570–3650 ppm in granodiorite are most likely caused by F bound in the residual phases i.e., apatite and titanite (Creaser et al. 1991) and abundant phlogopite. Moreover, the presence of titanite, without fluorite in the rapakivi-type quartz monzonite, suggests that A-type melt contained < 1 wt% F (Price et al. 1999). Nevertheless, F concentrations of < 1 wt% are sufficient to promote high HFSE contents, observed in the Pietkowo quartz monzonite, through complexing effects (Creaser et al. 1991). The presence of volatiles, such as F, results in lowering magma viscosity and could be responsible for the ascent of the granite magma through the crust (Clemens et al. 1986; Creaser et al. 1991), and ongoing formation of minerals,

both in the deep-seated magma chamber and at the final level of emplacement.

Therefore, we suggest that the rapakivi-type quartz monzonite was probably formed by crustal partial melting of the Late Paleoproterozoic dark-grey calc-alkalic granodiorite, giving A_2 -type granite magma, which subsequently crystallized during a two-step crystallization process. This accords with Anderson (1983), who proposed that crustal sources for this kind of A-type rock can vary from quartz diorite to granodiorite.

Regional context

The Proterozoic part of Fennoscandia was formed during the Svecofennian orogenic and post Svecofennian phases (Krzemińska et al. 2017; Skridlaite et al. 2021), ca. 300 Ma before the emplacement of A-type granitoid bodies; hence the term anorogenic (Condie 1991; Rämö and Haapala 1995; Bonin 2007) can refer also to the Pietkowo IG1 quartz monzonite intrusion emplaced at 1495–1491 Ma.

Considering the time of emplacement (Fig. 12), the Pietkowo IG1 quartz monzonite (1495–1491 Ma) is coeval with a few A-type granitoid bodies (i.e. Malbork IG1 (1499 Ma) and Kościerzyna IG1 (1499–1502 Ma)) in the vicinity of the Baltic Sea (Fig. 1B; Krzemińska et al. 2017, 2021) and slightly younger than 1525–1499 Ma A-type rocks of the MC (Dörr et al. 2002; Wiszniewska and Krzemińska 2021), as well as the prominent (1585 Ma) Riga batholith (Rämö et al. 1996) with its part in Gotland (Sundblad et al. 2021). Numerous small intrusive bodies and large batholiths of A-type granite composition are

Table 4 Regional compilation of ages of AMCG massifs in Fennoscandia

Location	Age [Ma]	Method	Reference
Poland			
Pietkowo	1495 ± 4 1492 ± 5 1491 ± 5	SIMS ^a	This study
<i>Kaszuby</i>			
Malbork	1499 ± 7	SIMS ^a	Krzemińska et al. (2017)
Kościerzyna	1498.8 ± 6		
Kościerzyna	1502 ± 10		
<i>Mazury</i>			
Filipów	1499 ± 7	SIMS ^a	Wiszniewska and Krzemińska (2021)
Łopuchowo	1513 ± 6		
Krasnopol	1516 ± 1	TIMS	Dörr et al. (2002)
Boksze	1512 ± 1		
Gołdap	1502 ± 2		
Lithuania			
Geluva	1445 ± 8	SIMS ^b	Skridlaite et al. (2007)
Rukai	1447 ± 5		
Žemaičių Naumiestis/1	1459 ± 3	TIMS	Motuzas et al. (2006)
Žemaičių Naumiestis/2	1462 ± 8		
Kabeliai	1505 ± 11	TIMS	Sundblad et al. (1994)
Lazdijai 1/1	1509 ± 8	SIMS ^b	Skridlaite et al. (2008)
Lazdijai 1/2	1522 ± 6		
South Sweden			
Noran	1469 ± 10	TIMS	Claesson and Kresten (1997)
Strömsbro	1500 ± 19	TIMS	Andersson (1997)
Ragunda	1505 ± 12 1514 ± 5	TIMS	Persson (1999)
Rödön	1497 ± 6	TIMS	Persson (1999), Andersson et al. (2001)
Nordsjö	1520 ± 3		Persson (1999), Andersson et al. (2001)
Mårdsjö	1524 ± 3		Persson (1999), Andersson et al. (2001)
Mullnåset	1526 ± 3		Persson (1999), Andersson et al. (2001)
Nordingrå	1578 ± 17		Welin and Lundqvist (1984), Persson (1999)
Russia			
Salmi	1540.6 ± 3.8 1538.9 ± 2.7 1538.5 ± 0.8 1537.7 ± 5 1538.7 ± 2.8 1537 ± 2.5 1534 ± 2 1533 ± 5	TIMS	Amelin et al. (1997)
South Finland			
Eurajoki	1571 ± 3	TIMS	Heinonen et al. (2010a)
Laitila	1573 ± 5		Vaasjoki (1996)
Åland	1575 ± 11	TIMS	Heinonen et al. (2010a)
Kolinummi	1576 ± 3	TIMS	Heinonen et al. (2010a)
Latvia			
Riga	1584 ± 7	TIMS	Rämö et al. (1996)
Estonia			
Märjamaa	1629 ± 7	TIMS	Rämö et al. (1996)
Naissaare	1624 ± 10		

Table 4 (continued)

Location	Age [Ma]	Method	Reference
Abja/1	1635 ± 7	TIMS	Kirs and Petersell (1994)
Abja/2	1622 ± 7		
South Finland			
Suomenniemi	1624 ± 7	SIMS ^b	Rämö and Mänttari (2015)
	1640 ± 9		
	1644 ± 4		
	1632 ± 5		
Ahvenisto	1633 ± 6	TIMS	Alviola et al. (1999)
Wiborg	1629 ± 4	SIMS ^b	Heinonen et al. (2017)
	1628 ± 3		
	1628 ± 2		
	1628 ± 3		
	1631 ± 4		
	1629 ± 4		
	1627 ± 3		
	1627 ± 3		
	1633 ± 2	TIMS	Rämö et al. (2014)

SIMS analyses performed on: ^a SHRIMP IIe/MC at the PGI-NRI (Warsaw, Poland)

^b Cameca IMS1270/1280 SIMS instrument of the Nordic high-resolution ion-microprobe facility (NORD-SIM) at the Swedish Museum of Natural History (Stockholm, Sweden)

well documented in southern Fennoscandia. Their compilation, including U–Pb ages together with whole-rock Nd isotopic data (Fig. 12), exhibits generally negative initial ϵ_{Nd} values, suggesting crustal contributions in the sources, whereas the large variation in their initial ϵ_{Nd} values (Fig. 12) implies some differences in the initial Sm/Nd ratio and Nd isotope composition, reflecting features of their local crustal sources, regardless of the time of the intrusion emplacement. The relatively young complex is the easternmost Salmi massif in Russian Karelia (ca. 1530–1540 Ma; Table 4; Amelin et al. 1997) which has initial ϵ_{Nd} values from -7.0 to -8.3 (Fig. 12; Neymark et al. 1994), whereas the older Riga rapakivi pluton (ca. 1585 Ma; Table 4; Rämö et al. 1996) has initial ϵ_{Nd} values from +0.3 to -4.8 (Fig. 12; Rämö et al. 1996). The same situations are observed in Sweden (e.g. the Rödön and Nordingrå massifs). The reason for this age distribution is unclear, but the belt-like geometry argues for a relationship to large-scale tectonic processes.

Most of AMCG suites are connected with previous deep-seated fault zones for their emplacement. Duchesne et al. (1999) argued that several anorthosite complexes, and the associated A-type granitoids, are commonly tied to former lithospheric-scale weakness zones, which may have favored their emplacement at higher crustal levels (cf. Dörr et al. 2002; Skridlaite et al. 2007). In the area of the southwestern EEC, the terrane boundaries, formed due to the Paleoproterozoic accretion of Fennoscandia, are suspected of being responsible for the magma uprising in the Mesoproterozoic.

A re-activation of transcurrent shear zones within uplifts and swells in a cratonic continental setting (Bonin 2007) remains one of typical tectonic context of A-type granite occurrences.

The major A-type rapakivi granitoids of the Finnish province, including the Salmi rapakivi intrusion in Russian Karelia, are associated with massif-type anorthosite. The MC (NE Poland) is also linked with at least three anorthosite massifs, forming a range of AMCG components (Dörr et al. 2002). The Paleoproterozoic collision-subduction episodes of the Svecofennian orogeny resulted in underthrusting of the lower crust to depths of ca. 40 km (Grad et al. 2009). Later upwelling of the asthenosphere could have caused the melting of the lower crust and mafic magmatism, represented by anorthosites of adjacent intrusion, which in turn could provide heat for generating the more felsic magma in the shallower crust. Thus, we suggest that the most plausible route for the Pietkowo IG1 rapakivi-type quartz monzonite ascent was the boundary between two crustal domains – the Mazowsze Domain and Belarus-Podlasie Granulite Belt pointed by the Białystok fault (Fig. 1B; cf. Krzemińska et al. 2017). The same fault zone could also have been responsible for the formation of the ~1.5 Ga Grodno Massif (Taran 2005), which lies on the NE extension of the Białystok fault, only 120 km to NE from the Pietkowo IG1 borehole. The positive magnetic and gravity anomalies recognized close to the Pietkowo IG1 intrusion may reflect the presence of the mafic component (e.g. anorthosites and gabbros) undrilled

so far (Fig. S1; Krzemińska et al. 2017) confirming the bimodal nature of this magmatism. Hence, the Mesoproterozoic rapakivi-type quartz monzonite of the Pietkowo IG1 borehole can be a component of the AMCG association in southernmost Fennoscandia. Demonstration of another massif from the unexposed area (Pietkowo IG1) supplements our state of knowledge about the specificity of rapakivi magmatism in Fennoscandia.

Conclusions

The study of the Pietkowo IG1 intrusion discovered within the hidden Late Paleoproterozoic part of the EEC documents (i) another occurrence of a Mesoproterozoic A-type granitoid of quartz monzonite composition with specific rapakivi-type texture, classified as weakly metaluminous, transient ferroan/magnesian and alkali-calcic magmatism, with elevated content of alkalis ($K_2O > Na_2O$). The high FeO/MgO ratio and elevated HFSE contents are compatible with other A-type granites, including examples from the Salmi (Russian Karelia) and Ahvenisto (S Finland) rapakivi batholiths. Pietkowo IG1 quartz monzonite show features of A_2 -type granite and belong to the magnetite-series. Pietkowo IG1 melt had to be generated under oxidizing conditions, as for the melts of MC granitoids. (ii) The Sm–Nd isotopic composition of the Pietkowo IG1 quartz monzonite is compatible with a lower crustal, early Proterozoic protolith (T_{DM} ages of 2.07–2.25 Ga) as is the case with a number of other rapakivi massifs (cf. Rämö and Haapala 1995) in Fennoscandia. (iii) The concordant age of the Pietkowo IG1 quartz monzonite indicates its emplacement at 1495–1491 Ma, although slightly older zircon cores (antecrysts) of 1513 ± 7 Ma imply a two-stage crystallization for the quartz monzonite. (iv) The Pietkowo IG1 rapakivi-type quartz monzonite is an example of, so far, the southernmost Mesoproterozoic massif of A-type affinity, belonging to the AMCG suites of Fennoscandia. (vi) It was connected with former lithospheric-scale weakness zones, between the east margin of the Mazowsze Domain and Belarus-Podlasie Granulite Belt pointed to by the Białystok fault.

Supplementary Information The online version contains supplementary material available at <https://doi.org/10.1007/s00710-022-00799-7>.

Acknowledgements The whole-rock chemical analyses were performed in the laboratories of the Bureau Veritas Commodities Ltd., Vancouver, Canada. The Nd isotopic analyses were carried out in the Isotope Laboratory of the Adam Mickiewicz University in Poznań, Poland. Thanks are addressed to Dominik Gurba for zircon separation, mount preparation and CL imaging and to Zbigniew J. Czupyt for SHRIMP He/MC calibration and support. Grazina Skridlaite, Krister Sundblad and Bernard Bonin are thanked for their constructive comments, which helped to improve the manuscript. Financial support was provided by the Polish Geological Institute-National Research Institute internal grant 62.9012.2060.00.0 to J.W. and the National

Science Centre Poland, through grant 2019/33/N/ST10/00944 to A.G. This contribution is dedicated to the memory of Ludmila Taran (1957–2021) – our friend, petrologist from Belarus, dealing with the issues of A-type granites.

Open Access This article is licensed under a Creative Commons Attribution 4.0 International License, which permits use, sharing, adaptation, distribution and reproduction in any medium or format, as long as you give appropriate credit to the original author(s) and the source, provide a link to the Creative Commons licence, and indicate if changes were made. The images or other third party material in this article are included in the article's Creative Commons licence, unless indicated otherwise in a credit line to the material. If material is not included in the article's Creative Commons licence and your intended use is not permitted by statutory regulation or exceeds the permitted use, you will need to obtain permission directly from the copyright holder. To view a copy of this licence, visit <http://creativecommons.org/licenses/by/4.0/>.

References

- Alviola R, Johanson BS, Rämö OT, Vaasjoki M (1999) The Proterozoic Ahvenisto rapakivi granite–massif-type anorthosite complex, southeastern Finland; petrography and U–Pb chronology. *Precambrian Res* 95(1–2):89–107
- Amelin YV, Larin AM, Tucker RD (1997) Chronology of multiphase emplacement of the Salmi rapakivi granite-anorthosite complex, Baltic Shield: implications for magmatic evolution. *Contrib Mineral Petrol* 127(4):353–368
- Anderson JL (1983) Proterozoic anorogenic granite plutonism of North America. In: Medaris LG Jr, Byers CW, Mickelson DM, Shanks WC (eds) *Proterozoic Geology; Selected Papers from an International Proterozoic Symposium*, vol 161. Geological Society of America Memoir, Boulder, pp 133–152
- Anderson JL, Morrison J (2005) Ilmenite, magnetite, and peraluminous Mesoproterozoic anorogenic granites of Laurentia and Baltica. *Lithos* 80(1–4):45–60
- Andersson UB (1997) The sub-Jotnian Strömsbro granite complex at Gävle, Sweden. *GFF* 119:159–167
- Andersson UB, Neymark LA, Billström K (2001) Petrogenesis of Mesoproterozoic (Subjotnian) rapakivi complexes of central Sweden: implications from U–Pb zircon ages, Nd, Sr and Pb isotopes. *Earth Environ Sci Trans R Soc Edinb* 92(3):201–228
- Appelquist K, Brander L, Johansson Å, Andersson UB, Cornell D (2011) Character and origin of variably deformed granitoids in central southern Sweden: Implications from geochemistry and Nd isotopes. *Geol J* 46(6):597–618
- Ashwal LD (2010) The temporality of anorthosites. *Canad Mineral* 48(4):711–728
- Bagiński B, Duchesne JC, Vander Auwera J, Martin H, Wiszniewska J (2001) Petrology and geochemistry of rapakivi-type granites from the crystalline basement of NE Poland. *Geol Quar* 45(1):33–52
- Black LP, Kamo SL, Allen CM, Aleinikoff JA, Davis DW, Korsch JR, Foudoulis C (2003) TEMORA 1: a new zircon standard for Phanerozoic U–Pb geochronology. *Chem Geol* 200:155–170
- Black LP, Kamo SL, Allen CM, Davis DW, Aleinikoff JN, Valley JW, Mundil R, Campbell H, Korsch RJ, Williams S, Foudoulis C (2004) Improved $^{206}Pb/^{238}U$ microprobe geochronology by the monitoring of a trace-element-related matrix effect; SHRIMP, ID–TIMS, ELA–ICP–MS and oxygen isotope documentation for a series of zircon standards. *Chem Geol* 205(1–2):115–140
- Bladh KL (1980) Rapakivi texture from the O'Leary Porphyry, Arizona (USA). *Bull Volcanol* 43(1):155–171
- Bogdanova SV, Gorbatshev R, Grad M, Janik T, Guterch A, Kozlovskaya E, Motuza G, Skridlaite G, Starostenko I, Taran L (2006)

- EUROBRIDGE: new insight into the geodynamic evolution of the East European Craton. In: Gee DG, Stephenson RA (eds) *European lithosphere dynamics*. Geological Society Memoirs 32(1), London, pp 599–625
- Bogdanova SV, Gorbatshev R, Skridlaite G, Soesoo A, Taran L, Kurlovich D (2015) Trans-Baltic Palaeoproterozoic correlations towards the reconstruction of supercontinent Columbia/Nuna. *Precambrian Res* 259:5–33
- Bonin B (2007) A-type granites and related rocks: evolution of a concept, problems and prospects. *Lithos* 97(1–2):1–29
- Boynnton WV (1984) Cosmochemistry of the rare earth elements: meteorite studies. In: Henderson P (ed) *Developments in geochemistry*. Elsevier, Amsterdam, pp 63–114
- Claesson S, Kresten P (1997) The anorogenic Noran intrusion—a Mesoproterozoic rapakivi massif in south-central Sweden. *GFF* 119(2):115–122
- Clemens JD, Holloway JR, White AJR (1986) Origin of an A-type granite; experimental constraints. *Am Mineral* 71(3–4):317–324
- Collins WJ, Beams SD, White AJR, Chappell BW (1982) Nature and origin of A-type granites with particular reference to Southeastern Australia. *Contrib Mineral Petrol* 80(2):189–200
- Condie KC (1991) Precambrian granulites and anorogenic granites: are they related? *Precambrian Res* 51:161–172
- Creaser RA, Price RC, Wormald RJ (1991) A-type granites: Assessment of a residual-source model. *Geology* 19(2):163–166
- Dadlez R, Grad M, Guterch A (2005) Crustal structure below the Polish Basin: is it composed of proximal terranes derived from Baltica? *Tectonophysics* 411(1–4):111–128
- Dall'Agnol R, Rämö OT, de Magalhães MS, Macambira MJB (1999a) Petrology of the anorogenic, oxidised Jamon and Musa granites, Amazonian Craton: implications for the genesis of Proterozoic A-type granites. *Lithos* 46(3):431–462
- Dall'Agnol R, Scaillet B, Pichavant M (1999b) An experimental study of a lower Proterozoic A-type granite from the Eastern Amazonian Craton, Brazil. *J Petrol* 40(11):1673–1698
- Dall'Agnol R, Teixeira NP, Rämö OT, Moura CA, Macambira MJ, de Oliveira DC (2005) Petrogenesis of the Paleoproterozoic rapakivi A-type granites of the Archean Carajás metallogenic province, Brazil. *Lithos* 80(1–4):101–129
- Dall'Agnol R, de Oliveira DC (2007) Oxidized, magnetite-series, rapakivi-type granites of Carajás, Brazil: implications for classification and petrogenesis of A-type granites. *Lithos* 93(3–4):215–233
- DePaolo DJ (1981) Neodymium isotopes in the Colorado Front Range and crust–mantle evolution in the Proterozoic. *Nature* 291(5812):193
- Dopieralska J (2003) Neodymium Isotopic Composition of Conodonts as a Palaeoceanographic Proxy in the Variscan Oceanic System. Dissertation, Justus-Liebig-University, Giessen, pp 111. <http://geb.uni-giessen.de/geb/volltexte/2003/1168/>. Accessed 8 Nov 2022
- Dörr W, Belka Z, Marheine D, Schastok J, Valverde-Vaquero P, Wiszniewska J (2002) U–Pb and Ar–Ar geochronology of anorogenic granite magmatism of the Mazury complex, NE Poland. *Precambrian Res* 119(1–4):101–120
- Duchesne JC, Liégeois JP, Vander Auwera J, Longhi J (1999) The crustal tongue melting model and the origin of massive anorthosites. *Terra Nova* 11(2–3):100–105
- Duchesne JC, Martin H, Bagiński B, Wiszniewska J, Vander Auwera J (2010) The origin of ferroan-potassic A-type granitoids: the case of the hornblende–biotite granite suite of the Mesoproterozoic Mazury complex, northeastern Poland. *Canad Mineral* 48(4):947–968
- Eby GN (1990) The A-type granitoids: a review of their occurrence and chemical characteristics and speculations on their petrogenesis. *Lithos* 26(1–2):115–134
- Eby GN (1992) Chemical subdivision of the A-type granitoids: petrogenetic and tectonic implications. *Geology* 20:641–644
- Eklund O, Shebanov AD (1999) The origin of rapakivi texture by sub-isothermal decompression. *Precambrian Res* 95(1–2):129–146
- Emslie RF (1991) Granitoids of rapakivi granite–anorthosite and related associations. *Precambrian Res* 51:173–192
- Frost BR, Barnes CG, Collins WJ, Arculus RJ, Ellis DJ, Frost CD (2001) A geochemical classification for granitic rocks. *J Petrol* 42(11):2033–2048
- Frost CD, Frost BR (1997) Reduced rapakivi-type granites: the tholeiite connection. *Geology* 25:647–650
- Frost CD, Frost BR, Chamberlain KR, Edwards BR (1999) Petrogenesis of the 1.43 Ga Sherman batholith, SE Wyoming, USA: a reduced, rapakivi-type anorogenic granite. *J Petrol* 40(12):1771–1802
- Fröjdö S, Andersson UB, Claesson S (1996) Nd isotope geochemistry of some mafic rocks and minerals associated with the Mesoproterozoic Åland and Nordingrå rapakivi batholiths, Fennoscandian shield. In: *International Conference on Proterozoic Evolution in the North Atlantic Realm*, Goose Bay, Labrador, Canada, pp 62–63
- Gawęda A, Krzemińska E, Wiszniewska J (2009) Granity typu A w kompleksie mazurskim— przyczynek do dyskusji o klasyfikacji granitów. *Prz Geol* 57(6):478–485 (in Polish)
- Grad M, Tiira T, ESC Working Group (2009) The Moho depth map of the European Plate. *Geophys J Int* 176(1):279–292
- Haapala I, Rämö OT (1990) Petrogenesis of the Proterozoic rapakivi granites of Finland. *Geol Soc Am Spec Pap* 246:275–286
- Haapala I, Rämö OT (1992) Tectonic setting and origin of the Proterozoic rapakivi granites of southeastern Fennoscandia. *Earth Environ Sci Trans R Soc Edinb* 83(1–2):165–171
- Heinonen AP, Andersen T, Rämö OT (2010a) Re-evaluation of rapakivi petrogenesis: Source constraints from the Hf isotope composition of zircon in the rapakivi granites and associated mafic rocks of southern Finland. *J Petrol* 51(8):1687–1709
- Heinonen AP, Rämö OT, Mänttari I, Johanson B, Alviola R (2010b) Formation and fractionation of high-Al tholeiitic magmas in the Ahvenisto rapakivi granite–massif-type anorthosite complex, southeastern Finland. *Canad Mineral* 48(4):969–990
- Heinonen AP, Rämö OT, Mänttari I, Andersen T, Larjamo K (2017) Zircon as a proxy for the magmatic evolution of Proterozoic ferroan granites; the Wiborg rapakivi granite batholith, SE Finland. *J Petrol* 58(12):2493–2517
- Ishihara S (1977) The magnetite-series and ilmenite-series granitic rocks. *Min Geol* 27:293–305
- Jacobsen SB, Wasserburg GJ (1980) Sm–Nd isotopic evolution of chondrites. *Earth Planet Sci Lett* 50:139–155
- Jiang N, Guo J, Zhai M (2011) Nature and origin of the Wenquan granite: Implications for the provenance of Proterozoic A-type granites in the North China craton. *J Asian Earth Sci* 42(1–2):76–82
- King PL, White AJR, Chappell BW, Allen CM (1997) Characterization and origin of aluminous A-type granites from the Lachlan Fold Belt, southeastern Australia. *J Petrol* 38:371–391
- Kirs J, Petersell V (1994) Age and geochemical character of plagiomicrocline granite veins in the Abja gabbro–dioritic massif. *Acta Comment Univ Tartu Math* 972:3–15
- Korja A, Lahtinen R, Nironen M (2006) The Svecofennian orogen: a collage of microcontinents and island arcs. *Geological Society Memoirs* 32(1), London, pp 561–578
- Krzemińska E, Williams I, Wiszniewska J (2005) A Late Paleoproterozoic (1.80 Ga) subduction-related mafic igneous suite from Lomza, NE Poland. *Terra Nova* 17(5):442–449
- Krzemińska E, Wiszniewska J, Williams IS, Dörr W (2007) Late Paleoproterozoic arc-related granites from the Mazowsze domain, NE Poland. In: Wiszniewska J (ed) *Kozłowski A. Granitoids in Poland*, Warsaw, pp 41–56
- Krzemińska E, Krzemiński L, Petecki Z, Wiszniewska J, Salwa S, Żaba J, Gaidzik K, Williams IS, Rosowiecka O, Taran L, Johansson Å,

- Pécskay Z, Demaiffe D, Grabowski J, Zieliński G (2017) Geological Map of Crystalline Basement in the Polish Part of the East European Platform 1:1000000. Polish Geological Institute, Warsaw
- Krzemińska E, Johansson ÅE, Krzemiński L, Wiszniewska J, Williams IS, Petecki Z, Salwa S (2021) Basement correlation across the southernmost Baltic Sea: Geochemical and geochronological evidence from onshore and offshore deep drill cores, northern Poland. *Precambrian Res* 362:106300
- Kubicki S, Ryka W (1982) Geological atlas of crystalline basement in Polish part of the East European Platform. Wydawnictwa Geologiczne, Warsaw, 24 tables
- Landenberger B, Collins WJ (1996) Derivation of A-type granites from a dehydrated charnockitic lower crust: evidence from the Chaelundi Complex, Eastern Australia. *J Petrol* 37(1):145–170
- Loiselle MC, Wones DR (1979) Characteristics and origin of anorogenic granites. *Geol Soc Am Abst with Programs* 11:468
- Lorenc MW, Wiszniewska J (1999) The Mazury complex: one magmatic influx or more. In: Wiszniewska J (ed) Between EUROBRIDGE and TESZ. Seventh EUROBRIDGE Workshop, Szelment-Suwalki, Poland. Abstracts, Warsaw, pp 66–68
- Ludwig KR (2003) User's manual for Isoplot/Ex version 3.00, a geochronological toolkit for Microsoft Excel. Berkeley Geochronology Center Berkeley Spec Publ 4:72
- Ludwig KR (2009) User's manual for SQUID 2.50. Berkeley Geochronology Center Berkeley Spec Publ 5:110
- Middlemost EA (1994) Naming materials in the magma/igneous rock system. *Earth Sci Rev* 37(3–4):215–224
- Motuz G, Čečys A, Kotov AB, Salnikova EB (2006) The Žemaičių Naumištis granitoids: new evidences for Mesoproterozoic magmatism in western Lithuania. *GFF* 128(3):243–254
- Narkiewicz N, Maksym A, Malinowski M, Grad M, Guterch A, Petecki Z, Probulski J, Janik T, Majdański M, Środa P, Czuba W, Gaczyński E, Jankowski L (2015) Transcurrent nature of the Teisseyre-Tornquist Zone in Central Europe – results of the POLCRUST-01 deep reflection seismic profile. *Int J Earth Sci* 104:775–796
- Neymark LA, Amelin VY, Larin AM (1994) Pb-Nd-Sr isotopic and geochemical constraints on the origin of the 1.54–1.56 Ga Salmi rapakivi granite – anorthosite batholith (Karelia, Russia). *Mineral Petrol* 50(1):173–193
- Patiño Douce AE (1997) Generation of metaluminous A-type granites by low-pressure melting of calc-alkaline granitoids. *Geology* 25:743–746
- Patiño Douce AE (1999) What do experiments tell us about the relative contributions of crust and mantle to the origin of granitic magmas? *Geol Soc London Spec Publ* 168(1):55–75
- Patiño Douce AE, Beard JS (1995) Dehydration-melting of biotite gneiss and quartz amphibolite from 3 to 15 kbar. *J Petrol* 36(3):707–738
- Pearce JA, Harris NBW, Tindle AC (1984) Trace element discrimination diagrams for the tectonic interpretation of granitic rocks. *J Petrol* 25:956–983
- Persson AI (1999) Absolute (U–Pb) and relative age determinations of intrusive rocks in the Ragunda rapakivi complex, central Sweden. *Precambrian Res* 95(1–2):109–127
- Poprawa P (2019) Geological setting and Ediacaran-Palaeozoic evolution of the western slope of the East European Craton and adjacent regions. *Ann Soc Geol Pol* 89:347–380
- Petecki Z, Rosowiecka O (2017) A new magnetic anomaly map of Poland and its contribution to the recognition of crystalline basement rocks. *Geol Quar* 61(4):934–945
- Price JD, Hogan JP, Gilbert MC, London D, Morgan GB (1999) Experimental study of titanite-fluorite equilibria in the A-type Mount Scott Granite: Implications for assessing F contents of felsic magma. *Geology* 27(10):951–954
- Rajesh HM (2000) Characterization and origin of a compositionally zoned aluminous A-type granite from South India. *Geol Mag* 137(3):291–318
- Rämö OT (1991) Petrogenesis of Proterozoic rapakivi granites and related basic rocks of southeastern Fennoscandia: Nd and Pb isotopic and general geochemical constraints. *Geol Surv Finland Bull* 355:161
- Rämö OT, Haapala I (1995) One hundred years of rapakivi granite. *Mineral Petrol* 52(3–4):129–185
- Rämö OT, Haapala I, Vaasjoki M, Yu JH, Fu HQ (1995) 1700 Ma Shachang complex, northeast China: Proterozoic rapakivi granite not associated with Paleoproterozoic orogenic crust. *Geology* 23(9):815–818
- Rämö OT, Huhma H, Kirs J (1996) Radiogenic isotopes of the Estonian and Latvian rapakivi granite suites: new data from the concealed Precambrian of the East European Craton. *Precambrian Res* 79:209–226
- Rämö OT, Dall'Agnol R, Macambira MJ, Leite AA, de Oliveira DC (2002) 188 Ga oxidized A-type granites of the Rio Maria region, eastern Amazonian craton, Brazil: positively anorogenic! *J Geol* 110(5):603–610
- Rämö OT, Turkki V, Mänttari I, Heinonen A, Larjamo KM, Lahaye Y (2014) Age and isotopic fingerprints of some plutonic rocks in the Wiborg rapakivi granite batholith with special reference to the dark wiborgite of the Ristisaari Island. *Bull Geol Soc Finl* 86:71–91
- Rämö OT, Mänttari I (2015) Geochronology of the Suomenniemi rapakivi granite complex revisited: Implications of point-specific errors on zircon U–Pb and refined λ_{87} on whole-rock Rb–Sr. *Bull Geol Soc Finl* 87:25–45
- Ryka W, Podemski M (1998) Geology of the Suwałki anorthosite massif (Northern Poland), vol 161. Prace Państwowego Instytutu Geologicznego, Warsaw
- Salminen J, Elming SÅ, Mertanen S, Wang C, Almqvist B, Moakhar MO (2021) Paleomagnetic studies of rapakivi complexes in the Fennoscandian shield—Implications to the origin of Proterozoic massif-type anorthosite magmatism. *Precambrian Res* 365:106406
- Shand SJ (1943) Classic A/CNK vs A/NK plot for discriminating metaluminous, peraluminous and peralkaline compositions. Hafner publishing co., New York
- Sharkov EV (2010) Middle-proterozoic anorthosite–rapakivi granite complexes: An example of within-plate magmatism in abnormally thick crust: Evidence from the East European Craton. *Precambrian Res* 183(4):689–700
- Skridlaite G, Bagiński B, Whitehouse M (2008) Significance of ~1.5 Ga zircon and monazite ages from charnockites in southern Lithuania and NE Poland. *Gondwana Res* 14(4):663–674
- Skridlaite G, Wiszniewska J, Duchesne JC (2003) Ferro-potassic A-type granites and related rocks in NE Poland and S Lithuania: west of the East European Craton. *Precambrian Res* 124(2–4):305–326
- Skridlaite G, Whitehouse M, Rimša A (2007) Evidence for a pulse of 1.45 Ga anorthosite–mangerite–charnockite–granite (AMCG) plutonism in Lithuania: implications for the Mesoproterozoic evolution of the East European Craton. *Terra Nova* 19(4):294–301
- Skridlaite G, Siliuskas L, Whitehouse MJ, Johansson Å, Rimša A (2021) On the origin and evolution of the 1.86–1.76 Ga Mid-Baltic Belt in the western East European Craton. *Precambrian Res* 367:106403
- Słaby E, Galbarczyk-Gąsiorowska L, Baszkiewicz A (2002) Mantled alkali-feldspar megacrysts from the marginal part of the Karkonosze granitoid massif (SW Poland). *Acta Geol Pol* 52(4):501–519
- Sun SS, McDonough WS (1989) Chemical and isotopic systematics of oceanic basalts: implications for mantle composition and processes. *Geol Soc Lond Sp Publ* 42(1):313–345

- Sundblad K, Mansfeld J, Motuza G, Ahl M, Claesson S (1994) Geology, geochemistry and age of a Cu-Mo-bearing granite at Kabeliai, southern Lithuania. *Mineral Petrol* 50:43–57
- Sundblad K, Salin E, Claesson S, Gyllencreutz R, Billström K (2021) The Precambrian of Gotland, a key for understanding the Proterozoic evolution in southern Fennoscandia. *Precambrian Res* 363:106321
- Taran L (2005) Gabbro-diorite-granodiorite-granite assemblage in Precambrian of NW Belarus. *Mineral Soc Pol Sp Pep* 26:85–88
- Vaasjoki M (1996) The Laitila rapakivi batholith revisited: new, more precise radiometric ages. In: Haapala I, Rämö OT, Kosunen P (eds) *The Seventh International Symposium on Rapakivi Granites and Related Rocks 24–26 July 1996*. University Press, Helsinki, p 82
- Wang Q, Zhu DC, Zhao ZD, Guan Q, Zhang XQ, Sui QL, Hu ZC, Mo XX (2012) Magmatic zircons from I-, S- and A-type granitoids in Tibet: Trace element characteristics and their application to detrital zircon provenance study. *J Asian Earth Sci* 53:59–66
- Welin E, Lundqvist T (1984) Isotopic investigations of the Nordingrå rapakivi massif, north-central Sweden. *GFF* 106(1):41–49
- Whalen JB, Currie KL, Chappell BW (1987) A-type granites: Geochemical characteristics, discrimination, and petrogenesis. *Contrib Mineral Petrol* 95:407–419
- Williams IS (1998) U-Th-Pb Geochronology by Ion Microprobe. In: McKibben MA, Shanks III WC, Ridley WI (eds) *Applications of microanalytical techniques to understanding mineralizing processes*, *Rev Econ Geol* 7. Society of Economic Geologist, Inc, Littleton, pp 1–35
- Williams IS, Krzemińska E, Wiszniewska J (2009) An extension of the Svecofennian orogenic province into NE Poland: evidence from geochemistry and detrital zircon from Paleoproterozoic paragneisses. *Precambrian Res* 172:234–254
- Wiszniewska J, Claesson S, Stein H, Vander Auwera J, Duchesne JC (2002) The north-eastern Polish anorthosite massifs: petrological, geochemical and isotopic evidence for a crustal derivation. *Terra Nova* 14(6):451–460
- Wiszniewska J, Kusiak MA, Krzemińska E, Dörr W, Suzuki K (2007) Mesoproterozoic AMCG granitoids in the Mazury complex, NE Poland—a geochronological update. In: Wiszniewska J (ed) Kozłowski A. *Granitoids in Poland*, Warsaw, pp 31–39
- Wiszniewska J, Krzemińska E (2021) Advances in geochronology in the Suwałki anorthosite massif and subsequent granite veins, northeastern Poland. *Precambrian Res* 361:106265
- Wones DR (1989) Significance of the assemblage titanite+ magnetite+ quartz in granitic rocks. *Am Mineral* 74(7–8):744–749

Publisher's note Springer Nature remains neutral with regard to jurisdictional claims in published maps and institutional affiliations.